



1 An Evaluation of the Performance of Sea-Bird Scientific's Autonomous SeaFET™:
2 Considerations for the Broader Oceanographic Community

3

4 Cale A. Miller^{1,3}, Katie Pocock², Wiley Evans², and Amanda L. Kelley^{1*}

5

6 1. College of Fisheries and Ocean Sciences, University of Alaska Fairbanks, Fairbanks, AK,
7 USA

8

9 2. Hakai Institute, Heriot Bay, BC, Canada

10

11 3. **Present address:** Department of Evolution and Ecology, College of Biological Sciences,
12 University of California Davis, CA, USA

13

14 *Correspondence to: Amanda L. Kelley (alkelley@alaska.edu)

15

16

17 Abstract

18

19 The commercially available Sea-Bird SeaFET™ provides an accessible way for a broad
20 community of researchers to study ocean acidification and obtain robust measurements of
21 seawater pH via the use of an *in situ* autonomous sensor. There are pitfalls, however, that have
22 been detailed in previous best practices for sensor care, deployment, and data handling. Here, we
23 took advantage of two distinctly different coastal settings to evaluate the Sea-Bird SeaFET™ and
24 examine the multitude of scenarios in which problems may arise confounding the accuracy of
25 measured pH. High-resolution temporal measurements of pH were obtained during 3- to 5-month
26 field deployments in three separate locations (two in south-central, Alaska, USA, and one British
27 Columbia, Canada) spanning a broad range of nearshore temperature and salinity conditions.
28 Both the internal and external electrodes onboard the SeaFET™ were evaluated against robust
29 benchtop measurements for accuracy utilizing either the factory calibration, an *in situ* single-
30 point calibration, or *in situ* multi-point calibration. In addition, two sensors deployed in parallel
31 in Kasitsna Bay, AK, USA, were compared for inter-sensor variability in order to quantify other
32 factors contributing to SeaFET™ intrinsic inaccuracies. Based on our results, the multi-point
33 calibration method provided the highest accuracy (< 0.025 difference in pH) of pH when
34 compared against benchtop measurements. Spectral analysis of time series data showed that
35 during spring in Alaskan waters, a range of tidal frequencies dominated pH variability, while
36 seasonal oceanographic conditions were the dominant driver in Canadian waters. Further, it is
37 suggested that spectral analysis performed on initial deployments may be able to act as an *a*
38 *posteriori* method to better identify appropriate calibration regimes. Based on this evaluation, we
39 provide a comprehensive assessment of the potential sources of uncertainty associated with
40 accuracy and precision of the SeaFETs™ electrodes.

41

42 1 Introduction

43

44 The intrusion of excess anthropogenic CO₂ into the global oceans—referred to as ocean
45 acidification (OA)—induces a series of geochemical reactions that increases seawater [H⁺]
46 (lowering pH) while concomitantly reducing the ocean's overall buffering capacity by reducing



47 the $[\text{CO}_3^{2-}]$ (Caldeira and Wickett, 2003; Orr et al., 2005). Due to more dynamic natural physical
48 and chemical processes in the coastal ocean, a differentiation exists between open-ocean
49 acidification and nearshore coastal acidification. Open-ocean acidification of surface waters is
50 predominately a function of equilibration with atmospheric $p\text{CO}_2$, thus increasing on yearly and
51 decadal timescales as continued burning of fossil fuels ensues (Hofmann et al., 2011; Orr et al.,
52 2005). Coastal acidification, however, can manifest on short time and space scales driven by
53 riverine input and its chemical constituents (e.g., organic carbon, nutrients, and organic
54 alkalinity), community metabolism and organization, tidal cycles, upwelling, and groundwater
55 input (Duarte et al., 2013; Sunda and Cai, 2012; Waldbusser and Salisbury, 2014), all of which
56 can act in conjunction with increasing atmospheric CO_2 , leading to more frequent, intense, and
57 longer-lasting acidification events (Hales et al., 2016; Harris et al., 2013). In the face of rapidly
58 changing coastal conditions, tracking and quantifying the progression of OA requires precise and
59 accurate measurements of carbonate chemistry over long periods of time; these can be achieved
60 by appropriately constraining the carbonate system by measuring at least two of the system's
61 parameters: total dissolved inorganic carbon (TCO_2), total alkalinity (TA), pH, and the partial
62 pressure of CO_2 ($p\text{CO}_2$). Despite the marked increase in OA research over the past decade
63 (Riebesell and Gattuso, 2015; Rudd, 2017), nearshore monitoring efforts—particularly in
64 estuarine waters—have been slow to ramp up, however, efforts are beginning to intensify as
65 technological advancements are made (Feely et al., 2010, 2016; Hales et al., 2016; Harris et al.,
66 2013; Newton et al., 2012; Waldbusser and Salisbury, 2014; Chan et al., 2017).

67
68 Acidification of Alaskan coastal waters is predicted to progress rapidly relative to other
69 regions within the next 50 years, and negatively impact the social-ecological structure of Alaskan
70 marine resources by disrupting the Alaska Native subsistence and commercial fisheries (Ekstrom
71 et al., 2015; Mathis et al., 2015b). The ocean waters present along the Alaskan coastline
72 experience chemical and physical drivers of seawater chemistry that are unique to this region.
73 The low seawater temperatures inherently have higher concentrations of dissolved CO_2 , and
74 chemical and physical oceanic processes unique to Alaskan waters such as sea ice melt, glacial
75 discharge, and benthic pelagic coupling across shallow shelves are likely to exacerbate
76 acidification in this region (Evans et al., 2014; Mathis et al., 2011a, 2011b, 2012). Recently, an
77 OA monitoring initiative has been setup by the Alaska Ocean Observing Network (AOOS) to
78 track and provide accessible material dedicated to acidification research in Alaskan waters
79 (<http://www.aos.org/alaska-ocean-acidification-network>). Along the Pacific coast of Alaska, a
80 robust benchtop system known as a Burke-o-Lator (BoL), which measures TCO_2 and $p\text{CO}_2$
81 either continuously in a flow-through environment or from discrete seawater samples (Bandstra
82 et al., 2006; Barton et al., 2012; Hales et al., 2016) has been installed in several locations,
83 including the OceansAlaska Shellfish Hatchery in Ketchikan, the Alutiiq Pride Shellfish
84 Hatchery in Seward (Evans et al., 2015), and at the Sitka Tribe of Alaska Environmental
85 Research Center (real-time data from Alaskan and other BoLs:
86 http://www.ipacoa.org/Explorer?action=oiw:fixed_platform). Nominal analytical uncertainty for
87 TCO_2 determinations from this system is 0.2% based on the reproducibility of sample and
88 certified reference material (CRM; provided by A. Dickson analyses). For $p\text{CO}_2$ determinations,
89 analytical uncertainty is 1.5% based on the inaccuracy of calculated CRM alkalinity relative to
90 the certified value. While the BoL has significant advantages for achieving robust OA
91 measurements in nearshore waters, the physical constraints of a benchtop system limit the spatial
92 dimension of which carbonate chemistry parameters can be measured. One potential resolution



93 to diminish the gap in coverage of OA monitoring is to utilize autonomous pH sensors, which are
94 far more versatile in their ability to monitor hard-to-reach areas.

95
96 Recent assessments regarding OA monitoring efforts have specifically highlighted the
97 benefits of accessibility by the commercially produced SeaFETTM pH sensor utilizing Honeywell
98 Durafet technology (Martz et al., 2015). The SeaFETTM was originally developed at the
99 Monterey Bay Aquarium Research Institute (Martz et al., 2010), but since has been
100 manufactured and distributed by Satlantic (<http://www.satlantic.com>), which is now incorporated
101 into Sea-Bird Scientific (<http://www.seabird.com>). The partnership between MBARI, Scripps
102 Institute of Oceanography, and Satlantic led the way for commercial availability of the
103 SeaFETTM, providing a ready-to-deploy-factory calibration, quick start manual, and user-friendly
104 interface. The first generation of SeaFETsTM (not distributed by Sea-Bird, but by Dr. Todd Martz
105 at Scripps Institute of Oceanography) have been deployed in numerous field studies and were
106 heavily scrutinized in order to provide robust best practices for appropriate calibration and
107 deployment procedures (Bresnahan et al., 2014; Hofmann et al., 2011; Kapsenberg and
108 Hofmann, 2016; Martz et al., 2010; Matson et al., 2011; Yu et al., 2011). More recent studies
109 have expanded the scope of SeaFETTM accuracy, inter-sensor variability, operator experience,
110 and multi-point calibration techniques (Gonski et al., 2018; Johnson et al., 2017; Kapsenberg et
111 al., 2017; McLaughlin et al., 2017). Given the multitude of information regarding SeaFETTM
112 performance, coalescing all the potential sources of uncertainty in measurements (e.g., inter-
113 sensor variability and calibration method) can be logistically challenging for non-experienced
114 oceanographers who now have access to the commercially available SeaFETsTM distributed by
115 Sea-Bird.

116
117 In this study, we aimed to take advantage of two distinct coastal settings in order to
118 deploy and evaluate the commercially available Sea-Bird SeaFETTM, and the potential
119 uncertainties that can arise with time series pH_t (total scale) measurements. For this evaluation,
120 SeaFETsTM were co-deployed side-by-side to quantify inter-sensor variability, discrepancies
121 were examined between factory calibration, *in situ* single-point calibration, and *in situ* multi-
122 point calibration pH_t values, and anomalous data associated with SeaFETTM conditioning times
123 were detailed and considered as potential sources of measurement inaccuracies. All evaluations
124 of SeaFETTM performance were under non-controlled source water conditions or by *in situ*
125 deployments. Three SeaFETsTM were deployed in coastal waters and were subjected to tidal
126 influences and freshwater input, while a fourth was compared to pH_t values derived from
127 measurements obtained by a BoL. Finally, a spectral analysis of the quality-controlled data was
128 performed in order to identify the driving mechanism of pH_t variability between these divergent
129 sites and consider possible un-accounted for calibration errors that could occur in dynamic
130 settings that might not be resolved using a specific calibration method.

131

132 **2 Methods**

133

134 **2.1 Apparatus: SeaFETTM**

135

136 The commercially available Sea-Bird SeaFETTM has retained the basic design of the original
137 SeaFETTM developed at MBARI (Martz et al., 2010). The SeaFETTM utilizes the ion sensitive
138 field effect transistor (ISFET) technology, and is outfitted with an internal Honeywell Durafet



139 and an external solid-state chloride selective electrode (Cl-ISE) along with an internal thermistor,
 140 which derives temperature using the (Steinhart and Hart, 1968) equation. The internal reference
 141 electrode is intrinsically insensitive to salinity over a tested range from 30 – 36 (Bresnahan et al.,
 142 2014), with recent work even suggesting near-ideal Nernstian response to salinity as low as ~9.0
 143 (Gonski et al., 2018). This is in converse to the chloride sensitive external electrode, which is
 144 salinity dependent. Both electrodes demonstrate exceptional stability over a range of moderate
 145 salinity (30 – 36) and broad temperature (-1 to 35 °C) (Bresnahan et al., 2014; Kapsenberg et al.,
 146 2015; Martz et al., 2014, 2010). The range of salinity sensitivity for the external electrode has
 147 even been extended down to 20, where it displays a near-ideal Nernst slope (Takeshita et al.,
 148 2014). Sea-Bird suggests that the external reference electrode provides the more accurate and
 149 stable pH_t measurement given that chloride concentration can be precisely determined from
 150 accurate salinity measurements. This is in agreement with previous research demonstrating that
 151 the external electrode has a more robust stability (Martz et al., 2010). In dynamic nearshore
 152 environments (e.g., estuaries with strong tidal and riverine fluxes), however, the pH_t derived
 153 from the internal electrode is recommended (Sea-Bird Scientific's Branham, C., pers. comm.)
 154 despite the potential of thermodynamic hysteresis (Martz et al., 2010). Bresnahan et al. (2014)
 155 demonstrated that the internal electrode is of the highest quality and under most scenarios
 156 remains nearly as stable as the external electrode—this was further corroborated by Gonski et al.
 157 (2018) with SeapHOx deployments in the Murderkill estuary, Delaware.

158 2.2 Calibration

159 Currently, three different calibration methods are present for the SeaFETTM: a factory pre-
 160 deployment single-point calibration, *in situ* single-point calibration, and an *in situ* multi-point
 161 calibration (Bresnahan et al., 2014; Gonski et al., 2018). To properly calculate pH_t from
 162 SeaFETTM voltage readings, an appropriate calibration coefficient is required. The applied
 163 calibration coefficients from the factory are a single-point, pre-deployment calibration. Given
 164 that a conditioning period is required for the SeaFETTM (Bresnahan et al., 2014), these
 165 coefficients are likely not adequate once the sensor becomes conditioned to the environment to
 166 which it is deployed. For the internal electrode, the new calibration coefficient k_{0i} can be
 167 determined as

$$171 \quad k_{0i} = -S_{Nernst} * pH_t + V_{int} - k_{2i} * T, \quad (1)$$

172 and k_{0e} for the external electrode

$$173 \quad k_{0e} = V_{ext} - pH_t + \log\left(1 + \frac{S_t}{K_s}\right) - 2 * \log(\gamma_{HCl}) - \log(Cl_T) * S_{nernst} + k_{2e} * T \quad (2)$$

174 where V_{FET} is the voltage from the electrode and k_2 is the temperature coefficient (dE^*/dT)
 175 applied to all SeaFETsTM (Martz et al., 2010). For detailed definitions of S_{nernst} and the salinity
 176 dependent constants γ_{HCl} (HCl activity coefficient), Cl_T (total chloride), S_T (total sulfate), and the
 177 HSO_4^- dissociation constant K_s (Dickson et al., 2007; Khoo et al., 1977) in equations 1 and 2, we
 178 refer readers to Martz et al. (2010), Bresnahan et al. (2014), and Sea-Bird Scientific SeaFETTM
 179 Product Manual 2.0.0. In the literature, SeaFETTM calibration coefficients have been denoted as
 180 E_{int}^* and E_{ext}^* (Martz et al. 2010, Bresnahan et al. 2014), however, for the purpose of this



184 evaluation—which specifically examines commercially available Sea-Bird SeaFETs™—the
185 adoption of k_0 and k_2 is in accordance with the preferred nomenclature from the manufacturer.

186

187

188 Unlike the factory pre-deployment single-point calibration, the *in situ* single-point
189 calibration occurs after the sensor has been deployed in the field. At the operator’s discretion, a
190 discrete sample will be collected in direct proximity to the deployed SeaFET™ at the same time
191 that the sensor is actively making a measurement, and then measured for pH_t at *in situ*
192 temperature and salinity. The known pH_t would then be used in the above equations as the “ pH_t ”
193 variable. Similar to the single-point *in situ* calibration, the multi-point calibration derives a series
194 of calibration coefficients over a short period of time that is long enough to capture environment
195 variability such as tidal fluxes, and then a single calibration coefficient is averaged. Both single-
196 point calibration methods—pre-deployment and *in situ*—appear to be suitable for fairly static
197 environmental conditions, whereas the multi-point *in situ* calibration is best suited for dynamic
198 nearshore environments (Bresnahan et al., 2014; Gonski et al., 2018).

198

199

200

2.3 SeaFET™ conditioning: test tank deployments

201

202

203

204

205

206

207

208

209

210

211

212

213

214

215

216

217

218

219

220

221

222

223

224

225

226

227

228

229

A series of three separate test tank deployments for three SeaFETs™_{395, 396, 397} were conducted in order to determine the conditioning period for each sensor. Initial sensor deployments took place in October 2016 at the Alutiiq Pride Shellfish Hatchery (APSH) in Seward, Alaska. Sensors were deployed for a duration of 72 hours in a flow-through 60 L tank where seawater taken from a depth of ~75 m in Resurrection Bay was sand-filtered, UV treated, and finally run through a 5 μm mesh. All three sensors were programmed with identical sampling settings (Table 1). The onboard internal thermistor was used to calculate temperature, and measurements of seawater salinity incoming to the hatchery were collected by a Sea-Bird Scientific SBE 45 MicroTSG Thermosalinograph that is paired with the BoL and are available on the Alaska Ocean Observing System (<http://portal.aos.org/real-time-sensors.php#map>). Factory calibration coefficients for the internal (k_{0i} , k_{2i}) and external (k_{0e} , k_{2e}) electrodes were retained when processing raw voltage data.

A second tank deployment for the same three SeaFETs™_{395, 396, 397} were deployed at the University of Alaska, Fairbanks, in the Ocean Acidification Research Center (OARC). Seawater collected from the APSH was delivered to the OARC test tank, ~370 L in a half-filled tank. Seawater in the tank was circulated continuously and covered to aid in the prevention of evaporation and photosynthesis. A co-deployed Sea-Bird SBE 16plusV2 SeaCAT (recently serviced by Sea-Bird) collected temperature and salinity readings every 5 minutes. SeaFETs™_{395, 396, 397} were deployed for a duration of nine days in continuous operation mode which forgoes the ability to set frames per burst; average number of reads was identical between all sensors (Table 1). From 1 – 4 November 2016, duplicate discrete bottle samples were collected in 250 ml glass bottles with screw caps at ~00:00 and 17:00 UTC per day. Bottle samples were preserved with 20 μl of saturated HgCl_2 and processed at a later date for TCO_2 and TA with a VINDTA 3C (Versatile Instrument for the Determination of total inorganic carbon and titration alkalinity). The VINDTA 3C has an uncertainty typically near 0.05% (Mathis et al., 2014, 2015a). Bottle sample pH_t was calculated using CO2SYS with known TCO_2 and TA using the constants provided by (Uppström, 1974) and (Lueker et al., 2000); derived pH_t was then compared against SeaFET™ sensor pH_t to test the accuracy of both internal and external



230 electrodes, assuming the discrete bottle samples were the “true pH” of the seawater. Upon
231 recovery, all SeaFETsTM_{395, 396, 397} were placed into polled mode and stored with wet caps filled
232 with tris buffer (salinity 34, pH 8.09 at room temperature, 25 °C). Again, the factory calibration
233 coefficients for the internal and external electrodes were retained when raw voltage was
234 processed. Since the SBE 16plusV2 sampled every 5 min, salinity and temperature measured by
235 the SBE at each 5-minute point was repeated for the following 4 minutes in order to calculate
236 continuous minute readings by SeaFETsTM_{395, 396, 397}.

237

238 A final test tank deployment of the SeaFETsTM_{395, 396, 397} at OARC was conducted after an
239 assumed adequate conditioning period of nine days (first OARC deployment). All three
240 SeaFETsTM_{395, 396, 397} had been set to polled mode after the end of the previous deployment and,
241 therefore, were sleeping for 83 days until this final seven day deployment. The sampling settings
242 were identical to the first OARC deployment for all three SeaFETsTM_{395, 396, 397} (Table 1). Similar
243 to the previous OARC tank deployment, a co-deployed Sea-Bird SBE 16plusV2 SeaCAT
244 collected temperature and salinity mirroring the SeaFET sampling interval of 3 hrs.

245

246 The internal thermistor of each SeaFETTM_{395, 396, 397} was tested for accuracy by comparing
247 its derived *in situ* temperature to that collected by the Sea-Bird SBE 16plusV2 during the test
248 tank deployments. The temperature difference between the internal thermistor and the SBE
249 16plusV2 was used to calculate the average and maximum discrepancy between the two
250 temperature readings. The temperature discrepancy was then applied to a combination of TA:
251 TCO₂ ratios over a range of salinity (20 – 35) in CO2SYS (constants: Uppström, 1974; Lueker et
252 al., 2000), which produced two different pH_t values. The difference between these two pH_t
253 values were, therefore, concluded to be a result of the temperature discrepancy.

254

255 2.4 SeaFETTM performance: field deployments

256

257 In late winter 2017—32 days post final tank deployment—SeaFETTM₃₉₇ was deployed at the
258 APSH and the two remaining sensors (SeaFETTM_{395, 396}) in Kasitsna Bay within greater
259 Kachemak Bay, Alaska (Fig. 1). At the APSH (60° 5' 55.59"N, 149° 26' 39.80"W), incoming
260 seawater from Resurrection Bay at a depth of 75 m is split before running through a series of
261 hatchery water filters so that an unfiltered line is run directly to the BoL. The incoming line to
262 the BoL was then split to feed an ~11.5 L conical tank housing the SeaFETTM₃₉₇ fit with the
263 copper bio-fouling guard; tank residence time was ~7.5 min. The SeaFETTM₃₉₇ at this location
264 was deployed on 6 March 2017 with a robust sampling setting (Table 1). Two calibration
265 methods were applied for this SeaFETTM₃₉₇, an *in situ* single-point calibration and an *in situ*
266 multi-point calibration. Both calibrations were performed 50 days after deployment on 25 April
267 2017 once the BoL had completed service maintenance. The single-point *in situ* calibration was
268 taken during midday tide transition in Resurrection Bay, while the multi-point *in situ* approach
269 used five (sensor sampling 3 h intervals) time points spanning an entire tidal cycle. The single-
270 point *in situ* calibration was used to derive k_{0i} for the internal electrode (eq. 1) and k_{0e} for the
271 external electrode (eq. 2). The multi-point *in situ* calibration followed the same formulations
272 with the difference being the final calibration coefficient calculated was the average of the five
273 independently calculated calibration coefficients. Three final pH_t values for the SeaFETTM₃₉₇
274 were, therefore, calculated based upon the different calibration coefficients (factory, single-point
275 and multi-point *in situ* calibration) and compared against the pH_t determined from continuous



276 $p\text{CO}_2$ measurements by the BoL and derived TA (TA-S equation, Evans et al. 2015) using
277 CO2SYS with constants provided by Uppström (1974) and Lueker et al. (2000). pH_t uncertainty
278 from the BoL using this combination of measured and derived parameters is 0.007 units based on
279 propagating the error of the BoL $p\text{CO}_2$ uncertainty reported above with the RMSE ($17 \mu\text{mol kg}^{-1}$)
280 of the regional TA-S relationship (Orr, et al., *in prep*).
281

282 Inter-sensor variability was examined between two SeaFETsTM_{395, 396} deployed off the
283 pier at the Kasitsna Bay laboratory in Kachemak Bay ($59^\circ 28' 6.71''\text{N}$, $151^\circ 33' 11.12''\text{W}$) ~ 1.5 m
284 from the bottom: depth at this location fluctuates between $\sim 7.5 - 16.8$ m (Fig. 1). On 18 March
285 2017—44 days post final tank deployment—SeaFETsTM_{395, 396} were attached to the pier piling
286 directly beside one another on a single mooring frame. Both SeaFETsTM were wrapped with pipe
287 tape to minimize biofouling and fit with their respective copper biofouling guards which had a
288 tributyltin plug attached to the inside of the guard. The sampling settings for both SeaFETsTM_{395,}
289 ₃₉₆ were identical to the one at the APSH (Table 1). Five discrete reference samples were taken in
290 duplicate: one sample on day of deployment (UTC: 3-18-17, 18:00), two samples 1-day post-
291 deployment (UTC: 19 March 2017, 03:00 and 15:00), and two samples 2- and 1-day pre-
292 recovery of the SeaFETsTM_{395, 396} (UTC 3 June 2017, 03:00; 6 June 2017, 03:00). Reference
293 samples were collected within 30 s of the instrument sampling time period via a diver's hand
294 Niskin, measured for temperature and salinity with a YSI 3100 conductivity instrument, stored in
295 250 ml glass bottles with screw caps, poisoned with 100 μl of saturated HgCl_2 , and secured with
296 teflon tape around the bottleneck threading and Parafilm wrapped on the outside of the cap.
297 Calibration samples were processed for TCO_2 and TA with a VINDTA 3C and pH_t calculated
298 using CO2SYS with the constants provided by Uppström (1974) and Lueker et al. (2000).
299 Salinity measurements collected by the Kachemak Bay National Estuarine Research Reserve
300 data sonde, 10 km SE of the deployed sensors ($59^\circ 26' 26.87''\text{N}$, $151^\circ 43' 15.21''\text{W}$), were used
301 along with the SeaFET'sTM internal thermistor readings to calculate pH_t from the raw voltage
302 data in order to capture representative environmental conditions providing relevance for the pH_t
303 time series in this location. A static salinity of 32 was also used for all calculations of pH_t as an
304 assessment of variability due to salinity measured from a data sonde 10 km away. A total of four
305 different pH_t values for both SeaFETsTM_{395, 396} were calculated based on calibration method
306 (factory pre-deployment single-point calibration and the *in situ* single-point) and conditioning:
307 either conditioned or non-conditioned to the environment. All calculated pH_t values from the
308 SeaFETsTM_{395, 396} were then compared against the remaining discrete reference bottle samples
309 not used for calibration. This was done in order to examine the accuracy and inter-sensor
310 variability difference between conditioned and non-conditioned to the environment electrodes.
311 Because the Kachemak Bay data sonde was located 10 km from the deployed SeaFETsTM_{395, 396},
312 the measured temperature and salinity from the discrete reference samples were used to
313 determine pH_t for the internal and external electrodes at those specific time points. That is,
314 sensor accuracy for these two SeaFETsTM_{395, 396} was only assessed with accurate temperature and
315 salinity values determined from the discrete bottle samples.
316

317 A fourth SeaFETTM₂₆₈ operated by the Hakai Institute was deployed on Environment
318 Canada's Sentry Shoal weather buoy in the Northern Strait of Georgia, BC, Canada: $49^\circ 54'$
319 $24.00''\text{N}$, $124^\circ 59' 5.99''\text{W}$ (Fig. 1). The Sentry Shoal mooring site is in a water depth of 15 m and
320 the SeaFETTM₂₆₈ was affixed at a depth of 1 m. A pre-deployment bucket test was conducted for
321 24 h at a sampling interval of 30 min with an average of 10 samples per frame and 30 frames per



322 burst from 28 – 29 June 2016. SeaFETTM₂₆₈ was outfitted with a copper housing guard and
 323 wrapped with copper tape. Sensor underwent two separate deployments, an initial deployment,
 324 and a redeployment (6 July and 27 August 2016) that occurred after the sensor was retrieved for
 325 cleaning and maintenance. Two separate calibration samples (taken in triplicate) were taken in
 326 accordance with each deployment, and occurred 13 and 7 days after each deployment (19 July
 327 and 2 September 2016). For each deployment, SeaFETTM₂₆₈ settings were similar to the others at
 328 the APSH and in Kasitsna Bay (Table 1). All calibration samples were taken in triplicate at a
 329 depth of 1 m via CTD and Niskin bottle castings and collected in 350 ml amber glass bottles with
 330 polyurethane-lined crimp-sealed metal caps and poisoned with 200 µl of saturated HgCl₂, and
 331 then processed for TCO₂ and pCO₂ with a BoL at the Hakai Institute's Quadra Island Field
 332 Station. The measured values were used to derive pH_t using CO2SYS with the constants
 333 provided by (Uppström, 1974) and (Lueker et al., 2000) in order to perform a single-point *in situ*
 334 calibration. Uncertainty in pH determinations from BoL pCO₂ and TCO₂ measurements was
 335 0.006 units. After SeaFETTM₂₆₈ deployment and calibration, a total of three, triplicate, reference
 336 sample sets were taken and processed for pH_t following the procedure used for calibration
 337 samples, then compared against SeaFET pH_t.

338 2.5 Quantifying pH_t and intrinsic sensor uncertainties

339

340 Calculating pH_t from the SeaFET'sTM raw voltage reading is dependent on temperature, salinity
 341 and an ideal 100% Nernstian response. The software application SeaFETcom permits the
 342 operator to automatically calculate pH_t by assigning the calibration coefficient either written to
 343 the sensor's header file or the one provided on the CD-ROM (these should be identical).
 344 Determination of final pH_t values from the first test tank deployment at the APSH were
 345 calculated by two different operators and two sources for the factory pre-deployment single-point
 346 calibration coefficients: header file and CD-ROM disc file. Aside from that exception, all other
 347 final pH_t values for the internal and external electrodes were calculated with the Mathworks
 348 software MATLAB (V. 2016a) and Microsoft excel (v. 2016) using the following equations for
 349 the internal electrode

350

$$351 \quad pH_{int} = \frac{V_{FET|INT} - k_{0i} - k_{2i} * T}{S_{nernst}}, \quad (3)$$

352 and the external electrode

$$353 \quad pH_{ext} = \frac{V_{FET|EXT} - k_{0e} - k_{2e} * T}{S_{nernst}} + \log(Cl_T) + 2 * \log(\gamma_{HCl}) - \log\left(1 + \frac{S_t}{K_s}\right) \quad (4)$$

354 where V_{FET} is the voltage from the electrode and k₂ is the temperature coefficient (dE*/dT)
 355 applied to all SeaFETsTM (Martz et al. 2010). Again, for detailed definitions of S_{nernst} and the
 356 salinity dependent constants γ_{HCl} (HCl activity coefficient), Cl_T (total chloride), S_t (total sulfate),
 357 and the HSO₄⁻ dissociation constant K_s (Khoo et al. 1977, Dickson et al. 2007) in equations 3 and
 358 4, we refer readers to Martz et al. (2010), Bresnahan et al. (2014), and Sea-Bird Scientific
 359 SeaFETTM Product Manual 2.0.0.

360 2.5.1 Sensor uncertainty

361 The overall accuracy (i.e., integrated uncertainties) of every SeaFETTM sensor was evaluated by



362 quantifying all sources of potential uncertainty when calculating a final pH_t from the SeaFETTM.
363 The pH_t uncertainty introduced by calibration method was calculated as the absolute difference
364 between the “true pH_t ” and the final sensor pH_t derived from either factory calibration, the
365 single-point *in situ* calibration, or multi-point *in situ* calibration. The “true pH_t ” was calculated
366 using CO2SYS dissociation constants by Lueker et al., (2000) and Uppström, (1974) with
367 measured TCO_2 and TA via the VINDTA 3C, TCO_2 and pCO_2 measured by the BoL for discrete
368 samples (e.g., SeaFETTM₂₆₈), and pCO_2 and TA (TA-S equation, Evans et al. 2015) for
369 continuous samples (SeaFETTM₃₉₇). A one-way analysis of variance (ANOVA) and the root
370 mean square error (RMSE) were run and calculated in order to compare the pH_t values from both
371 electrodes on SeaFETTM₃₉₇ across calibration methods against the pH_t values from the BoL. The
372 BoL at the APSH sampled every 5 min which produced 256 comparable sample points with a
373 time alignment disparity that ranged from 0 – 120 s against SeaFETTM₃₉₇. The potential pH_t
374 uncertainty based on the thermistor was calculated by using the absolute difference between the
375 thermistor derived temperature and that measured by the SBE 16plusV2 (T_{diff}) from the OARC
376 test tank deployments and the Kasitsna Bay SeaFETsTM_{395, 396} against the Seldovia data sonde 10
377 km away. Finally, an average inter-sensor variability uncertainty term was calculated as the
378 difference between the two SeaFETsTM_{395, 396} deployed side-by-side in Kasitsna Bay after a
379 single-point *in situ* calibration was performed. All uncertainty terms were calculated and collated
380 based on our evaluations from the Alaska deployed SeaFETsTM_{395, 396, 397}, while SeaFETTM₂₆₈
381 deployed at Sentry Shoal was only included when determining the accuracy uncertainty term.
382 Due to the disparity between reference samples for the Kasitsna Bay SeaFETsTM_{395, 396} and
383 Sentry Shoal SeaFETTM₂₆₈ (two discrete reference samples) to that at the ASPH SeaFETTM₃₉₇
384 (256 reference samples), only the average calculated difference (SeaFETTM pH_t – “true pH_t ”) for
385 each calibration method and electrode was used from the APSH SeaFETTM₃₉₇ and then collated
386 with the other reference points from the Kasitsna Bay and Sentry Shoal SeaFETsTM_{395, 396, 268}.

387 2.5.2 pH_t time series analysis

388

389 Final time series analysis was examined in the time and frequency domain using the Mathworks
390 software MATLAB (V. 2016a). Power spectral density was determined via Welch’s method
391 using the pwelch function in MATLAB. Time series data was resampled and linearly
392 interpolated in order to compensate for the missing data points that occurred when sensors
393 arbitrarily stopped sampling.

394

395 3 Results

396

397 3.1 Test tank and field conditions

398

399 Finalized (i.e., calibrated) pH_t values from the first test tank deployment produced two different
400 values, of which each was dependent on whether the calibration coefficient from the header file
401 or the disc file was selected, the result was a difference of ~0.0011 units for both the internal and
402 external electrodes. Because sensors were stored in tris buffer that lacked the addition of bromide
403 between tank deployments and before field deployments, an environmental conditioning period
404 was required for each of the Alaska SeaFETsTM_{395, 396, 397} once submerged in their respective
405 field sites. Thus, any determination of SeaFETTM pH_t accuracy and conditioning period from



406 tank deployments were inconclusive and will not be considered henceforth. No SeaFETsTM_{395, 396,}
407 _{397, 268} displayed signs of biofouling or low battery power upon recovery.

408

409 SeaFETTM₃₉₇ deployed in parallel with the BoL at the APSH experienced a tank failure
410 on 8 April 2017 resulting in the sensor's emergence for 24 h. In addition, missing temperature
411 and salinity values resulted in gaps of pH_t measurements over the entire deployment. The BoL
412 experienced flow control issues when initial deployment occurred on 6 March 2017 and was not
413 online until 18 April 2017 but, then, operated nearly consistently until 24 May 2017. All pH_t and
414 temperature comparisons were, therefore, made beginning on 18 April 2017.

415

416 Due to the *in situ* environmental conditioning period of the Kasitsna Bay SeaFETsTM_{395,}
417 _{396,} calibration was performed using the initial reference sample collected on 18 March 2017,
418 03:00 UTC and again with the reference sample collected on 3 June 2017, 03:00 UTC. Due to
419 high variance between duplicate reference samples (SD: 0.08 pH_t) on 19 March 2017, 15:00
420 UTC, this reference was discarded and not used for comparison or calibration. The Sentry Shoal
421 SeaFETTM₂₆₈ underwent one maintenance and cleaning procedure, including a battery change,
422 during the ~5-month deployment (Table 1). One calibration sample (19 July 2016) and one
423 reference sample (9 November 2016) were averaged from duplicate rather than triplicate
424 replicates due to large variance from one of the replicate samples. The reference sample taken on
425 23 August 2016, 17:00 UTC was discarded as temperature and salinity data were missing and
426 SeaFETTM₂₆₈ pH_t could not be calculated. The final reference sample (UTC: 9 November 2016,
427 17:05) was taken 5 min after SeaFETTM₂₆₈ sampled on 9 November 2016, 17:00 UTC.

428

429 **3.2 Thermistor response: test tank deployment**

430

431 The internal thermistor amongst the SeaFETsTM_{395, 396, 397} had a difference of less than 0.2 °C
432 over the entirety of the second and third tank deployments. All thermistor derived temperature
433 values had good alignment with the SBE 16plusV2 temperature, and consistently recorded a
434 slightly higher temperature. The discrepancy between the thermistor temperature and
435 SBE16plusV2 was minimal, and reached a maximum of 0.378 (logged by SeaFETTM₃₉₅) during
436 any time over all tank deployments. The average discrepancy, however, was ~0.21 °C when
437 averaging across all SeaFETsTM_{395, 396, 397} and all times.

438

439 **3.3 Field performance**

440

441 SeaFETTM₃₉₇ deployed alongside the BoL appeared stable throughout its entire deployment and
442 tracked the pH_t derived from the BoL well (Fig. 2). Errant spikes were present from both
443 electrodes throughout periods before 18 April 2017, which were a result of plumbing changes
444 that occurred to the APSH incoming seawater. On 10 April 2017 the internal thermistor, BoL
445 temp, and BoL salinity fluctuated by 3 °C and 14, respectively, over a 12 h period. These
446 anomalies were removed from analysis. Salinity remained relatively stable throughout the rest of
447 the deployment and ranged from 30.0 – 32.1. The pH_t uncertainty (SeaFETTM – “true” pH_t)
448 decreased, and the accuracy of the SeaFET'sTM₃₉₇ internal electrode improved once the *in situ*
449 single-point and multi-point calibrations were performed with a RMSE decreasing from 0.5455
450 pH_t units under factory calibration, 0.0361 pH_t units for *in situ* single-point calibration and
451 0.0273 pH_t units for the *in situ* multi-point calibration. The external electrode also improved



452 accuracy with *in situ* single-point and multi-point calibrations with an RMSE of 0.1077 under
453 factory calibration, 0.0390 for *in situ* single-point calibration and 0.0388 for the *in situ* multi-
454 point calibration (Fig. 2). There was a significant difference in the reduction of the pH_t
455 uncertainty for both the internal and external electrodes when utilizing *in situ* single-point and
456 multi-point calibration coefficients compared to the factory calibration coefficients (Table 2). In
457 addition, there was a significant decrease in the pH_t uncertainty when using the *in situ* multi-
458 point calibration coefficients rather than the *in situ* single-point method for the internal electrode,
459 but not for the external electrode (Table 2). The pH_t uncertainty of the internal electrode
460 decreased from 0.0294 units with an *in situ* single-point calibration to 0.0224 units after an *in*
461 *situ* multi-point calibration. It should be noted that the time alignment disparity which ranged
462 from 0 – 120 s is not considered a significant source of discrepancy as only 4 sample points out
463 of the 256 comparable points were > 0.03 units (i.e., only 4 comparable points greater than the
464 average pH_t uncertainty found after calibration) between any one 5 min sample taken by the
465 BoL. The internal thermistor of SeaFETTM₃₉₇ tracked the recorded BoL temperature trend fairly
466 (Fig. 3), but had a greater magnitude discrepancy than its test tank deployment (~ 0.21 °C). On
467 average, the thermistor temperature had an absolute difference of 2.83 °C (SD 0.35) from 18
468 April 2017 – 6 June 2017, which would result in a pH_t uncertainty of ~ 0.044 units. SeaFETTM₃₉₇
469 was not fully submerged in the conical tank leaving the top portion susceptible to air temperature
470 fluctuations which could have affected the thermistor readings.

471

472 The SeaFETsTM_{395, 396} in Kasitsna Bay improved their accuracy after an *in situ* single-
473 point calibration was performed (Fig. 4), however, this was only the case when sensors were not
474 conditioned as calibration performed after the conditioning period reduced accuracy (Fig. 5). It
475 should be noted that only the pH_t recorded by both SeaFETsTM_{395, 396} at times of the reference
476 samples had precise salinity and temperature (temperature and salinity recorded with reference
477 sample rather than thermistor derived temperature) measurements as all other measurements
478 were calculated from salinity measured by the data sonde 10 km away, and with temperature
479 derived from the onboard thermistor. The pH_t recorded by the external electrode at a fixed
480 salinity displayed little to no variance relative to pH_t calculated with data sonde salinity (< 0.02
481 pH_t difference: average whether conditioned or non-conditioned to environment). The average
482 pH_t uncertainty from both SeaFETsTM_{395, 396} reduced by approximately half for the internal
483 electrode when not conditioned to the environment after an *in situ* single-point calibration was
484 performed (0.1072 and 0.1394 to 0.0475 and 0.0741 units, respectively), while the external
485 electrode improved only minimally from 0.0988 and 0.0963 to 0.0610 and 0.0894 units,
486 respectively (Fig. 4). When *in situ* single-point calibration was performed after the
487 SeaFETsTM_{395, 396} were conditioned (i.e., calibrated with reference sample taken on 4 June 2017,
488 03:00 UTC), the pH_t uncertainty for the internal electrode reduced only minimally from factory
489 calibration: 0.1072 and 0.1394 to 0.0896 and 0.1240 units, respectively (Fig. 5a, b). Conversely,
490 the pH_t error for the external electrode increased from 0.0988 and 0.0963 to 0.1011 and 0.1480,
491 respectively (Fig 5c, d).

492

493 Both SeaFETsTM_{395, 396} displayed low inter-sensor variability for the internal electrode,
494 and high for the external electrode after *in situ* single-point calibration was performed on sensors
495 not conditioned to the environment (Fig. 6, gray circles). The mean anomaly between both
496 SeaFETsTM_{395, 396} internal electrodes was 0.0525 units, whereas the external mean anomaly was
497 0.145 units. When measurements taken before the sensor was conditioned to the environment



498 (blue shaded region Fig. 6) were removed from analysis, the mean anomaly changed by < 0.006
499 units for both electrodes. Inter-sensor variability for both electrodes once conditioned, and after
500 *in situ* single-point calibration, was < 0.05 units: 0.0409 and 0.0461 units for the internal and
501 external electrodes, respectively (Fig. 6, black circles). When measurements recorded before the
502 sensors were conditioned to the environment were removed (blue shaded region Fig. 10), the
503 anomaly decreased further, < 0.015 units for both electrodes.

504

505 Thermistor readings on both SeaFETsTM_{395, 396} tracked the temperature at the Seldovia
506 site well, however errant spikes occurred around 18 April 2017 and again around 10 May 2017,
507 and continued till the end of the deployment (Fig. 7). The absolute average difference between
508 the thermistor values and the Seldovia data sonde was 0.281 °C (SD 0.295), nearly identical to
509 the difference displayed during the test tank deployments, average 0.21 °C.

510

511 At Sentry Shoal, temperature and salinity seasonally fluctuated and ranged from $8.71 -$
512 21.8 °C and $23.4 - 29.4$, respectively. There was no clear distinction in greater accuracy between
513 the internal and external electrodes after *in situ* single-point calibration was performed. While the
514 external electrode did display a lower pH_t average uncertainty, this was based on only two
515 reference points, one of which had a time discrepancy of 5 min (9 November 2016, 17:05 UTC).
516 Only two reference samples were comparable against SeaFETTM₂₆₈ pH_t due to the loss of salinity
517 and temperature data on 23 August 2016, 17:00 UTC. Reference samples on 26 September 2016
518 and 9 November 2016 were, therefore, compared using the new calibration coefficients
519 determined after redeployment on 27 August 2016. The average pH_t uncertainty was < 0.0115
520 units for both electrodes (Fig. 8) compared to average pH_t uncertainties of 0.0244 and 0.0560
521 units for the internal and external electrodes, respectively, if initial calibration coefficients from
522 19 July 2016 were retained. The low pH_t uncertainty (< 0.0137 units) determined after the *in situ*
523 single-point calibration, however, was still greater than the average pH_t uncertainty under factory
524 calibration: < 0.005 units for both electrodes (Fig 8).

525

526 3.4 Spectral analysis

527

528 All SeaFETsTM_{395, 396, 397, 268} displayed a mixed semi-diurnal tidal response during all field
529 deployments (Fig. 9). SeaFETsTM_{395, 396} at Kasitsna Bay had a stronger amplitude response at a
530 frequency of two cycles d^{-1} , whereas SeaFETTM₃₉₇ had a greater amplitude at one cycle d^{-1} (Fig.
531 9a, c, d). All three SeaFETsTM_{395, 396, 397} in Alaskan waters had a strong amplitude signal of 1
532 cycle every 21 days, with an addition signal of one cycle every three days for SeaFETTM₃₉₇. The
533 amplitude signal for SeaFETTM₃₉₇ shifted depending on source of measurement (BoL, internal or
534 external electrode), however, all measurement sources followed the same frequency pattern (Fig
535 9a). SeaFETTM₂₆₈ displayed a strong signal at a frequency of zero as well as at one and two
536 cycles d^{-1} (Fig 9a).

537

538 3.5 Intrinsic uncertainty and accuracy

539

540 Among the calculated potential sources of uncertainty in pH_t , inter-sensor variability (difference
541 between SeaFET'sTM pH_t) and sensor accuracy produced the greatest uncertainty discrepancies
542 for the internal and external electrodes under factory calibration (Fig. 10). The pH_t uncertainty
543 (i.e., overall sensor accuracy) for the internal electrode reduced a greater degree than the external



544 electrode at every ordinal calibration method: factory, *in situ* single-point, to *in situ* multi-point
545 calibration (Fig. 10). This was not the case for the external electrode, however, as the overall pH_t
546 accuracy was greater when factory calibration was used compared to an *in situ* single-point
547 calibration was performed after the sensor was conditioned. The thermistor uncertainty (i.e.,
548 uncertainty when calculating pH_t based on the thermistor temperature rather than a more accurate
549 temperature gauge) produced a pH_t uncertainty of 0.0044 units, and was based on the recorded
550 values by SeaFETsTM_{395, 396}. Even though the temperature-derived values from the thermistor of
551 SeaFETsTM_{395, 396} were compared against a data sonde 10 km away, the average T_{diff} values were
552 consistent with the T_{diff} calculated from the test tank deployments (within 0.07°C) and, therefore,
553 provided an adequate resolution to determine a thermistor uncertainty value.

554

555 4 Discussion

556

557 Obtaining accurate and precise measurements of pH in nearshore coastal waters is crucial for
558 understanding changing trends, dynamics, and current baselines of acidification in these—
559 “susceptible to change”—marine domains. For dynamic nearshore systems, the current standard
560 of OA weather (carbonate chemistry variability on timescales of days to months) accuracy
561 should have an uncertainty no greater than 0.02 pH units according to the Global Ocean
562 Acidification Observing Network (Newton et al. 2015). Previous evaluations of the SeaFETTM
563 sensor package have demonstrated accuracy for both electrodes to be better than 0.02 pH units,
564 with a range between 0.01 – 0.04 units for the internal electrode in more dynamic environments
565 (Bresnahan et al., 2014; Gonski, 2018; Martz et al., 2010). Based on our findings, we observed
566 an accuracy range of 0.009 – 0.148 pH_t units after sensors were conditioned and *in situ* single-
567 point or multi-point calibrations were performed for the internal and external electrodes. This
568 range decreased when SeaFETsTM_{395, 396} from Kasitsna Bay were calibrated with reference
569 samples taken at initial deployment (i.e., non-conditioned to environment). For SeaFETTM₃₉₇, the
570 internal electrode’s accuracy was nearly identical to that of the external electrode after an *in situ*
571 multi-point calibration (Fig. 2), suggesting that the internal electrode can produce a highly
572 precise pH_t measurement comparable to the BoL with an accuracy meeting the standards of the
573 OA weather measurements (Newton et al. 2015). This is not to suggest that the SeaFETTM can
574 replace the BoL, particularly because the BoL can capture multiple carbonate chemistry
575 measurements thereby fully constraining the system and identifying potential decoupling of the
576 carbonate system in estuarine waters (Bandstra et al., 2006; Hales et al., 2016). Nonetheless, the
577 SeaFETTM can provide an accurate measurement of pH_t in nearshore waters when SeaFETTM
578 operation is executed with high precision.

579

580 SeaFETsTM_{397, 268} deployed at the APSH and at Sentry Shoal displayed the lowest
581 uncertainty and greatest precision of pH_t measurements (Fig. 2 and 8). In both instances, the
582 SeaFETsTM_{397, 268} were adequately conditioned (i.e., subjected to *in situ* conditions for ~50 days)
583 before calibration was performed. The greater overall accuracy displayed by the SeaFETTM₂₆₈ at
584 Sentry Shoal may be due to the fact that the sensor was exposed to *in situ* conditions for a longer
585 period of time and re-calibrated multiple times to the same environment. Further, calibration and
586 reference sample pH_t was derived from TCO_2 and $p\text{CO}_2$ processed by the BoL at Sentry Shoal
587 and from $p\text{CO}_2$ (also measured by BoL) and the TA-salinity relationship (Evans et al. 2015) at
588 the APSH. It is unclear as to why the sensor accuracy of both Kasitsna Bay SeaFETsTM_{395, 396}
589 was substantially less than the SeaFETsTM_{397, 268} at the APSH or Sentry Shoal. A potential reason



590 for the low accuracy may be that sensors were calibrated at a reference point that was extreme
591 relative to the time series pH_t signal—that is, calibrated at a time of high variability. In this case,
592 performing an *in situ* multiple-point calibration could have reduced the uncertainty and increased
593 the accuracy. While previous studies have found that collection and preservation of calibration
594 and reference samples can result in a decrease in accuracy depending on operator experience
595 (McLaughlin et al., 2017), the operator in this study was considered to have substantial
596 experience conducting such operations used in this evaluation. In addition, given the increased
597 pH_t variability over a short temporal period—which can be seen at the end of the Kasitsna Bay
598 deployment (Fig. 4 and 5)—and the low discrepancy between duplicate reference samples, the
599 former reasoning (i.e., calibrated to an extreme reference point) is a more reasonable explanation
600 for the reduced accuracy by the Kasitsna Bay SeaFETsTM_{395, 396} than operator experience. We re-
601 iterate here that reference sample temperature and salinity were used to calculate SeaFETTM pH_t
602 at the time points in which sensor pH_t and reference sample pH_t were compared, thus salinity
603 was not a confounding factor.

604

605 Despite the lower accuracy of the Kasitsna Bay SeaFETsTM_{395, 396}, the two sensors
606 provided a better insight of inter-sensor variability for non-conditioned to the environment and
607 conditioned electrodes. After *in situ* single-point calibration for conditioned sensors, the average
608 inter-sensor variability decreased for the internal electrode by ~80%, and >300% for the external
609 electrode (Fig. 6). The inter-sensor variability reported here was still greater than previous
610 findings (Kapsenberg et al., 2017), however, the comparison made in this study was done in the
611 field compared to controlled laboratory conditions as in Kapsenberg et al. (2017). And while
612 non-homogenized water could lead to anomalies in pH_t measurements by the Kasitsna Bay
613 SeaFETsTM_{395, 396}, it is unlikely that water was consistently non-homogenized over the entirety of
614 a deployment at a distance of < 20 cm (distance between electrodes on each SeaFETTM).
615 Furthermore, due to the dynamic nature of Kachemak Bay, where the tidal exchanges are
616 extreme, averaging 4.73 m, it is unlikely that micro-heterogeneity of seawater is the driving force
617 behind the observed differences in pH_t measurements that were observed between SeaFETsTM_{395,}
618 ₃₉₆. There was a tradeoff for a decrease in inter-sensor variability, as the *in situ* single-point
619 calibration performed after sensors were conditioned resulted in a decrease in accuracy compared
620 to an *in situ* single-point calibration performed for sensors not conditioned to the environment. It
621 should be noted that we do not consider salinity to be a potential source of uncertainty for inter-
622 sensor variability because the pH_t difference using data sonde salinity compared to a fixed
623 salinity resulted in an anomaly of < 0.005 units.

624

625 The Sentry Shoal SeaFETTM₂₆₈ had the lowest average pH_t uncertainty for both electrodes
626 after *in situ* single-point calibration was performed, however, these were still greater than the pH_t
627 uncertainty determined using the factory calibration coefficients. This specific example
628 highlights two possibilities: (1) the role of inter-sensor variability, as this may be a coincidental
629 case given the uncertainty observed when quantifying inter-sensor variability, and (2) the
630 influence of variance within a calibration sample set. For the case of SeaFETTM₂₆₈, the replicate
631 calibration samples collected on 19 July 2016 and 2 September 2016 for the first and second
632 deployments had standard deviations of 0.016 and 0.005 pH_t units, respectively. For instances of
633 generally close agreement between factory and *in situ* calibrated data, the variance in the
634 calibration sample set may contribute to better agreement between factory calibrated sensor pH_t
635 data and average discrete sample pH_t measurements. It should also be noted that pre-deployment



636 calibration can provide highly accurate measurements by the Honeywell Durafet (internal
637 electrode), however, matching exact conditions to those at the field site are necessary (Johnson et
638 al., 2017), and this was not likely the case for the factory provided calibration coefficients.
639

640 The evaluation of SeaFETTM performance presented here corroborates and contrasts with
641 previous studies examining the overall accuracy and precision of pH_t measurements made by
642 these oceanographic instruments. While the accuracy of two SeaFETsTM_{397, 268} fall well within
643 the range determined from previous studies, the accuracy of SeaFETsTM_{395, 396} at Kasitsna Bay
644 lay outside the bounds of what has been report in the primary literature (Bresnahan et al., 2014;
645 Gonski et al., 2018; Johnson et al., 2017; Kapsenberg et al., 2017; Martz et al., 2010).
646 Nevertheless, it is relevant to report the potential uncertainties possible when operating
647 SeaFETsTM as a multitude of factors can influence the overall accuracy (e.g., operator, sample
648 preservation, electrode conditioning, calibration measurements), therefore, the potential
649 uncertainties calculated in this study represent the upper limit of an average uncertainty compiled
650 from four different SeaFETsTM (Fig. 10). The utility of such an analysis provides a confidence in
651 SeaFETTM operation, and highlights all the potential uncertainties that need to be considered
652 when deploying the sensors in the field. For example, we have included a thermistor uncertainty
653 term determined from the test tank and field deployments of the Alaska SeaFETsTM_{395, 396, 397},
654 even though a suitable solution around this issue would be to apply an offset to the thermistor
655 temperature given it was compared to more robust temperature measurements conducted before
656 field deployment. It should be noted, that in this case, the thermistor uncertainty observed from
657 SeaFETTM₃₉₇ against the BoL was excluded as the lag time between thermistor response and tank
658 residence time likely confounded the comparison. The potential pH_t uncertainties presented here
659 should serve as a guide for SeaFETTM operators in order to better understand the source of an
660 uncertainty and take the necessary steps to improve SeaFETTM measurements. Bresnahan et al.
661 (2014) acknowledged that relying on the SeaFETTM for an accurate pH measurement should be
662 viewed cautiously if additional biogeochemical sensors are not co-deployed to cross-validate the
663 stability and accuracy of the SeaFET'sTM electrodes, therefore, being fully aware of all the
664 potential uncertainties presented here will only further aid SeaFETTM operators.
665

666 The time series data provided by the SeaFETTM deployments in this study have expanded
667 the scope of spatial pH_t variability along the North American west coast. The SeaFETsTM_{395, 396}
668 deployed in Kasitsna Bay provide some of the first high temporal resolution measurements of
669 pH_t in this region. During this spring deployment, it appears that semi-diurnal tidal fluctuations
670 are the dominant contributor to pH_t variability with an additional cycle occurring every 21 days
671 coinciding with the seasonal spring and neap tides (Fig. 9). The SeaFETTM₂₆₈ at Sentry Shoal
672 also displays a strong pH_t response to the semi-diurnal mixed tidal cycle. A strong signal is also
673 present at a frequency of zero, and is likely a result of the long, across-season, time series. That
674 is, over the course of the entire deployment which went from summer into late fall, seasonal
675 drivers of pH_t (e.g., decrease in water temperature) confounded repetitive frequency patterns. In
676 addition, Sentry Shoal may have a weaker tidal signature relative to other pH_t modulators that do
677 not follow a cyclical pattern such as water mass intrusion, inconsistent metabolic cycles from the
678 end of summer into the fall season, and a shift to the rainy season.
679

680 As an elaboration on the power spectral density analysis, we suggest this form of
681 frequency analysis can be utilized to better understand the system in which a SeaFETTM is



682 deployed, thus informing the operator as to what the drivers of their system are, and when to
683 calibrate the sensor. It is possible that in a highly dynamic setting, the sensor could re-condition
684 over time periods not resolved in a multi-point calibration sampling scheme, and this could
685 enhance sensor inaccuracies. For example, in Kasitsna Bay, a strong semi-diurnal tide cycle was
686 present, so upon redeployment in this area, if possible, the best calibration approach would be an
687 *in situ* multi-point calibration between the M2 cycle. Alternatively, if the system is not driven by
688 a strong tidal signature (e.g., non-coastal region), an *in situ* single point calibration may be a
689 reasonable approach.

690

691 **5 Conclusion**

692

693 The following evaluation of the Sea-Bird SeaFETTM helped elucidate the overall
694 accuracy and highlighted the potential uncertainties and pitfalls of operating and obtaining pH_t
695 measurements by the internal and external electrode pair. We found that the internal electrode
696 provided the more robust measurement in nearshore estuarine waters when an *in situ* multi-point
697 calibration was performed (Fig. 10). The quantified potential pH_t uncertainty is based
698 specifically on our findings, whereas further results may minimize this uncertainty given
699 additional evaluations. However, the results here provide an upper limit of the pH_t uncertainty
700 that may be observed when operating a Sea-Bird SeaFETTM. Further, high temporal resolution
701 pH_t measurements in nearshore Canadian and Alaskan waters provide a better understanding of
702 the drivers modulating pH on short timescales. Given the application, the Sea-Bird SeaFETTM
703 can provide a reliable and accurate pH_t measurement which can be utilized to broaden the
704 coverage of understanding pH variability in nearshore and open-ocean waters.

705

706 **Acknowledgments**

707 The authors would like to thank Jeff Hetrick and Jacqueline Ramsey at the Alutiiq Pride
708 Shellfish Hatchery for providing their facilities and services for this evaluation. We would also
709 like to thank Angela Doroff at the Kasitsna Bay laboratory for providing facilities for SeaFETTM
710 deployments. Funding for this project was provided in part by the University of Alaska
711 Fairbanks College of Fisheries and Ocean Sciences. WE and KP thank the Pacific Salmon
712 Foundation and Environment Canada for providing the platform for deploying SeaFET 268, the
713 University of Alaska Fairbanks Ocean Acidification Research Center for the long-term use of
714 SeaFET 268, and the Tula Foundation for supporting their efforts with this work.

715

716

717 **References**

718 Bandstra, L., Hales, B. and Takahashi, T.: High-frequency measurements of total CO₂: Method
719 development and first oceanographic observations, *Mar. Chem.*, 100(1–2), 24–38,
720 doi:10.1016/j.marchem.2005.10.009, 2006.

721 Barton, A., Hales, B., Waldbusser, G. G., Langdon, C. and Feely, R. A.: The Pacific oyster,
722 *Crassostrea gigas*, shows negative correlation to naturally elevated carbon dioxide levels:
723 Implications for near-term ocean acidification effects, *Limnol. Oceanogr.*, 57(3), 698–710,
724 doi:10.4319/lo.2012.57.3.0698, 2012.



- 725 Bresnahan, P. J., Martz, T. R., Takeshita, Y., Johnson, K. S. and LaShomb, M.: Best practices for
726 autonomous measurement of seawater pH with the Honeywell Durafet, *Methods Oceanogr.*, 9,
727 44–60, doi:10.1016/j.mio.2014.08.003, 2014.
- 728 Caldeira, K. and Wickett, M. E.: Anthropogenic carbon and ocean pH, *Nature*, 425(6956), 365–
729 365, doi:10.1038/425365a, 2003.
- 730 Chan, F., Barth, J. A., Blanchette, C. A., Byrne, R. H., Chavez, F., Cheriton, O., Feely, R. A.,
731 Friederich, G., Gaylord, B., Gouhier, T., Hacker, S., Hill, T., Hofmann, G., McManus, M. A.,
732 Menge, B. A., Nielsen, K. J., Russell, A., Sanford, E., Sevdjian, J. and Washburn, L.: Persistent
733 spatial structuring of coastal ocean acidification in the California Current System, *Sci. Rep.*, 7(1),
734 2526, doi:10.1038/s41598-017-02777-y, 2017.
- 735 Dickson, A. G., Sabine, C. L. and Christian, J. R.: Guide to Best Practices for Ocean CO₂
736 Measurements., Report, North Pacific Marine Science Organization. [online] Available from:
737 <http://www.oceandatapactices.net:80/handle/11329/249>, 2007.
- 738 Duarte, C. M., Hendriks, I. E., Moore, T. S., Olsen, Y. S., Steckbauer, A., Ramajo, L.,
739 Carstensen, J., Trotter, J. A. and McCulloch, M.: Is Ocean Acidification an Open-Ocean
740 Syndrome? Understanding Anthropogenic Impacts on Seawater pH, *Estuaries Coasts*, 36(2),
741 221–236, doi:10.1007/s12237-013-9594-3, 2013.
- 742 Ekstrom, J. A., Suatoni, L., Cooley, S. R., Pendleton, L. H., Waldbusser, G. G., Cinner, J. E.,
743 Ritter, J., Langdon, C., van Hooijdonk, R., Gledhill, D., Wellman, K., Beck, M. W., Brander, L.
744 M., Rittschof, D., Doherty, C., Edwards, P. E. T. and Portela, R.: Vulnerability and adaptation of
745 US shellfisheries to ocean acidification, *Nat. Clim. Change*, 5(3), 207–214,
746 doi:10.1038/NCLIMATE2508, 2015.
- 747 Evans, W., Mathis, J. T. and Cross, J. N.: Calcium carbonate corrosivity in an Alaskan inland
748 sea, *Biogeosciences*, 11(2), 365–379, doi:10.5194/bg-11-365-2014, 2014.
- 749 Evans, W., Mathis, J. T., Ramsay, J. and Hetrick, J.: On the Frontline: Tracking Ocean
750 Acidification in an Alaskan Shellfish Hatchery, *PLOS ONE*, 10(7), e0130384,
751 doi:10.1371/journal.pone.0130384, 2015.
- 752 Feely, R. A., Alin, S. R., Newton, J., Sabine, C. L., Warner, M., Devol, A., Krembs, C. and
753 Maloy, C.: The combined effects of ocean acidification, mixing, and respiration on pH and
754 carbonate saturation in an urbanized estuary, *Estuar. Coast. Shelf Sci.*, 88(4), 442–449,
755 doi:10.1016/j.ecss.2010.05.004, 2010.
- 756 Feely, R. A., Alin, S. R., Carter, B., Bednaršek, N., Hales, B., Chan, F., Hill, T. M., Gaylord, B.,
757 Sanford, E., Byrne, R. H., Sabine, C. L., Greeley, D. and Juranek, L.: Chemical and biological
758 impacts of ocean acidification along the west coast of North America, *Estuar. Coast. Shelf Sci.*,
759 183, Part A, 260–270, doi:10.1016/j.ecss.2016.08.043, 2016.
- 760 Gonski, S. F., Cai, W.-J., Ullman, W. J., Joesoef, A., Main, C. R., Pettay, D. T. and Martz, T. R.:
761 Assessment of the suitability of Durafet-based sensors for pH measurement in dynamic estuarine



- 762 environments, *Estuar. Coast. Shelf Sci.*, 200(Supplement C), 152–168,
763 doi:10.1016/j.ecss.2017.10.020, 2018.
- 764 Hales, B., Suhrbier, A., Waldbusser, G. G., Feely, R. A. and Newton, J. A.: The Carbonate
765 Chemistry of the “Fattening Line,” Willapa Bay, 2011–2014, *Estuaries Coasts*, 1–14,
766 doi:10.1007/s12237-016-0136-7, 2016.
- 767 Harris, K. E., DeGrandpre, M. D. and Hales, B.: Aragonite saturation state dynamics in a coastal
768 upwelling zone, *Geophys. Res. Lett.*, 40(11), 2720–2725, doi:10.1002/grl.50460, 2013.
- 769 Hofmann, G. E., Smith, J. E., Johnson, K. S., Send, U., Levin, L. A., Micheli, F., Paytan, A.,
770 Price, N. N., Peterson, B., Takeshita, Y., Matson, P. G., Crook, E. D., Kroeker, K. J., Gambi, M.
771 C., Rivest, E. B., Frieder, C. A., Yu, P. C. and Martz, T. R.: High-Frequency Dynamics of Ocean
772 pH: A Multi-Ecosystem Comparison, *Plos One*, 6(12), e28983,
773 doi:10.1371/journal.pone.0028983, 2011.
- 774 Johnson, K. S., Plant, J. N., Coletti, L. J., Jannasch, H. W., Sakamoto, C. M., Riser, S. C., Swift,
775 D. D., Williams, N. L., Boss, E., Haentjens, N., Talley, L. D. and Sarmiento, J. L.:
776 Biogeochemical sensor performance in the SOCCOM profiling float array, *J. Geophys. Res.-*
777 *Oceans*, 122(8), 6416–6436, doi:10.1002/2017JC012838, 2017.
- 778 Kapsenberg, L., Bockmon, E. E., Bresnahan, P. J., Kroeker, K. J., Gattuso, J.-P. and Martz, T.
779 R.: Advancing Ocean Acidification Biology Using Durafet® pH Electrodes, *Front. Mar. Sci.*, 4,
780 doi:10.3389/fmars.2017.00321, 2017.
- 781 Kapsenberg, L. and Hofmann, G. E.: Ocean pH time-series and drivers of variability along the
782 northern Channel Islands, California, USA, *Limnol. Oceanogr.*, 61(3), 953–968,
783 doi:10.1002/lno.10264, 2016.
- 784 Kapsenberg, L., Kelley, A. L., Shaw, E. C., Martz, T. R. and Hofmann, G. E.: Near-shore
785 Antarctic pH variability has implications for the design of ocean acidification experiments, *Sci.*
786 *Rep.*, 5, srep09638, doi:10.1038/srep09638, 2015.
- 787 Khoo, K. H., Ramette, R. W., Culberson, C. H. and Bates, R. G.: Determination of hydrogen ion
788 concentrations in seawater from 5 to 40.degree.C: standard potentials at salinities from 20 to
789 45%, *Anal. Chem.*, 49(1), 29–34, doi:10.1021/ac50009a016, 1977.
- 790 Lueker, T. J., Dickson, A. G. and Keeling, C. D.: Ocean pCO₂ calculated from dissolved
791 inorganic carbon, alkalinity, and equations for K-1 and K-2: validation based on laboratory
792 measurements of CO₂ in gas and seawater at equilibrium, *Mar. Chem.*, 70(1–3), 105–119,
793 doi:10.1016/S0304-4203(00)00022-0, 2000.
- 794 Martz, T., Send, U., Ohman, M. D., Takeshita, Y., Bresnahan, P., Kim, H.-J. and Nam, S.:
795 Dynamic variability of biogeochemical ratios in the Southern California Current System,
796 *Geophys. Res. Lett.*, 41(7), 2496–2501, doi:10.1002/2014GL059332, 2014.
- 797 Martz, T. R., Connery, J. G. and Johnson, K. S.: Testing the Honeywell Durafet® for seawater
798 pH applications, *Limnol. Oceanogr. Methods*, 8(5), 172–184, doi:10.4319/lom.2010.8.172, 2010.



- 799 Martz, T. R., Daly, K. L., Byrne, R. H., Stillman, J. H. and Turk, D.: Technology for ocean
800 acidification research: needs and availability, *Oceanography*, 28(2), 40–47, 2015.
- 801 Mathis, J. T., Cross, J. N. and Bates, N. R.: Coupling primary production and terrestrial runoff to
802 ocean acidification and carbonate mineral suppression in the eastern Bering Sea, *J. Geophys.*
803 *Res. Oceans*, 116(C2), C02030, doi:10.1029/2010JC006453, 2011a.
- 804 Mathis, J. T., Cross, J. N. and Bates, N. R.: The role of ocean acidification in systemic carbonate
805 mineral suppression in the Bering Sea, *Geophys. Res. Lett.*, 38(19), L19602,
806 doi:10.1029/2011GL048884, 2011b.
- 807 Mathis, J. T., Pickart, R. S., Byrne, R. H., McNeil, C. L., Moore, G. W. K., Juranek, L. W., Liu,
808 X., Ma, J., Easley, R. A., Elliot, M. M., Cross, J. N., Reisdorph, S. C., Bahr, F., Morison, J.,
809 Lichendorf, T. and Feely, R. A.: Storm-induced upwelling of high pCO₂ waters onto the
810 continental shelf of the western Arctic Ocean and implications for carbonate mineral saturation
811 states, *Geophys. Res. Lett.*, 39(7), L07606, doi:10.1029/2012GL051574, 2012.
- 812 Mathis, J. T., Cross, J. N., Monacci, N., Feely, R. A. and Stabeno, P.: Evidence of prolonged
813 aragonite undersaturations in the bottom waters of the southern Bering Sea shelf from
814 autonomous sensors, *Deep-Sea Res. Part II-Top. Stud. Oceanogr.*, 109, 125–133,
815 doi:10.1016/j.dsr2.2013.07.019, 2014.
- 816 Mathis, J. T., Cross, J. N., Evans, W. and Doney, S. C.: Ocean Acidification in the Surface
817 Waters of the Pacific-Arctic Boundary Regions, *Oceanography*, 28(2), 122–135,
818 doi:10.5670/oceanog.2015.36, 2015a.
- 819 Mathis, J. T., Cooley, S. R., Lucey, N., Colt, S., Ekstrom, J., Hurst, T., Hauri, C., Evans, W.,
820 Cross, J. N. and Feely, R. A.: Ocean acidification risk assessment for Alaska’s fishery sector,
821 *Prog. Oceanogr.*, 136, 71–91, doi:10.1016/j.pocean.2014.07.001, 2015b.
- 822 Matson, P. G., Martz, T. R. and Hofmann, G. E.: High-frequency observations of pH under
823 Antarctic sea ice in the southern Ross Sea, *Antarct. Sci.*, 23(6), 607–613,
824 doi:10.1017/S0954102011000551, 2011.
- 825 McLaughlin, K., Dickson, A., Weisberg, S. B., Coale, K., Elrod, V., Hunter, C., Johnson, K. S.,
826 Kram, S., Kudela, R., Martz, T., Negrey, K., Passow, U., Shaughnessy, F., Smith, J. E., Tadesse,
827 D., Washburn, L. and Weis, K. R.: An evaluation of ISFET sensors for coastal pH monitoring
828 applications, *Reg. Stud. Mar. Sci.*, 12, 11–18, doi:10.1016/j.rsma.2017.02.008, 2017.
- 829 Newton J.A., Feely R. A., Jewett E. B., Williamson P. & Mathis J.
830 2015. Global Ocean Acidification Observing Network: Requirements and Governance Plan.
831 Second Edition, GOA-ON, http://www.goa-on.org/docs/GOA-ON_plan_print.pdf.
832
- 833 Newton, J., Devol, A., Alford, M., Mickett, J., Sabine, C. and Sutton, A.: Nanoos Contributions
834 to Understanding Ocean Acidification, *J. Shellfish Res.*, 31(1), 327–327, 2012.
- 835 Orr, J. C., Fabry, V. J., Aumont, O., Bopp, L., Doney, S. C., Feely, R. A., Gnanadesikan, A.,
836 Gruber, N., Ishida, A., Joos, F., Key, R. M., Lindsay, K., Maier-Reimer, E., Matear, R., Monfray,



- 837 P., Mouchet, A., Najjar, R. G., Plattner, G. K., Rodgers, K. B., Sabine, C. L., Sarmiento, J. L.,
838 Schlitzer, R., Slater, R. D., Totterdell, I. J., Weirig, M. F., Yamanaka, Y. and Yool, A.:
839 Anthropogenic ocean acidification over the twenty-first century and its impact on calcifying
840 organisms, *Nature*, 437(7059), 681–686, doi:10.1038/nature04095, 2005.
- 841 Orr, J. C., J.-M. Epitalon, A. G. Dickson, and J.-P. Gattuso: Routine uncertainty propagation for
842 the marine carbon dioxide system, *Marine Chemistry, in prep.*
843
- 844 Riebesell, U. and Gattuso, J.-P.: Lessons learned from ocean acidification research, *Nat. Clim.*
845 *Change*, 5(1), 12–14, doi:10.1038/nclimate2456, 2015.
- 846 Rudd, M. A.: What a Decade (2006–15) Of Journal Abstracts Can Tell Us about Trends in
847 Ocean and Coastal Sustainability Challenges and Solutions, *Front. Mar. Sci.*, 4,
848 doi:10.3389/fmars.2017.00170, 2017.
- 849 Steinhart, J. S. and Hart, S. R.: Calibration curves for thermistors, *Deep Sea Res. Oceanogr.*
850 *Abstr.*, 15(4), 497–503, doi:10.1016/0011-7471(68)90057-0, 1968.
- 851 Sunda, W. G. and Cai, W.-J.: Eutrophication Induced CO₂-Acidification of Subsurface Coastal
852 Waters: Interactive Effects of Temperature, Salinity, and Atmospheric P-CO₂, *Environ. Sci.*
853 *Technol.*, 46(19), 10651–10659, doi:10.1021/es300626f, 2012.
- 854 Takeshita, Y., Martz, T. R., Johnson, K. S. and Dickson, A. G.: Characterization of an Ion
855 Sensitive Field Effect Transistor and Chloride Ion Selective Electrodes for pH Measurements in
856 Seawater, *Anal. Chem.*, 86(22), 11189–11195, doi:10.1021/ac502631z, 2014.
- 857 Uppström, L. R.: The boron/chlorinity ratio of deep-sea water from the Pacific Ocean, *Deep Sea*
858 *Res. Oceanogr. Abstr.*, 21, 161–162, doi:10.1016/0011-7471(74)90074-6, 1974.
- 859 Waldbusser, G. G. and Salisbury, J. E.: Ocean Acidification in the Coastal Zone from an
860 Organism's Perspective: Multiple System Parameters, Frequency Domains, and Habitats,
861 *Annu. Rev. Mar. Sci.*, 6(1), 221–247, doi:10.1146/annurev-marine-121211-172238, 2014.
- 862 Yu, P. C., Matson, P. G., Martz, T. R. and Hofmann, G. E.: The ocean acidification seascape and
863 its relationship to the performance of calcifying marine invertebrates: Laboratory experiments on
864 the development of urchin larvae framed by environmentally-relevant pCO₂/pH, *J. Exp. Mar.*
865 *Biol. Ecol.*, 400(1–2), 288–295, doi:10.1016/j.jembe.2011.02.016, 2011.
- 866
867
868
869
870
871
872
873
874
875



876 **Table 1.** Deployment regime of all four SeaFETs™ including deployment location, date, and
 877 calibration methods performed. *Non-controlled source water pumped directly from
 878 Resurrection Bay, AK, USA.
 879

| Location (Tank or Field) | Date | SeaFET™ ID | Average reads frame ⁻¹ | Frames Burst ⁻¹ | Sampling Freq. (min) | Calibration method |
|------------------------------|--|---------------|--------------------------------------|-------------------------------|-------------------------|--------------------------------------|
| APSH — <i>Tank</i> | 5 – 8 October 2016 | 395, 396, 397 | 1 | 10 | 5 | Factory |
| OARC — <i>Tank</i> | 26 October – 3 November 2016 | 395, 396, 397 | 3 | — | Continuous | Factory |
| OARC — <i>Tank</i> | 26 January – 1 February 2017 | 395, 396, 397 | 1 | 10 | 180 | Factory |
| APSH <i>Field*</i> | 5 March – 6 June 2017 | 397 | 10 | 30 | 180 | Factory, SP and MP <i>in situ</i> |
| Kachemak Bay <i>Field</i> | 18 March – 4 June 2017 | 395, 396 | 10 | 30 | 180 | Factory, SP <i>in situ</i> |
| Sentry Shoal <i>Field</i> | 6 July – 23 August, 27 August – 28 November 2016 | 268 | 10 | 30 | 30 | Factory, SP <i>in situ</i> |

880
881
882
883
884
885
886
887
888
889
890
891
892
893
894
895
896
897
898
899
900
901
902
903
904
905
906



907 **Table 2.** One-way Analysis of variance comparing the pH_t error (SeaFETTM pH_t – BoL pH_t)
 908 across calibration methods for both the internal and external electrodes onboard SeaFETsTM₂₆₈ at
 909 Sentry Shoal (factory calibration and *in situ* single-point calibration) and SeaFETTM₃₉₇ at the
 910 Alutiiq Pride Shellfish Hatchery (factory calibration, *in situ* single-point calibration, and *in situ*
 911 multi-point calibration). Bold type denotes statistical significance.

| Site | Electrode | Source | SS | df | MS | F | p-value |
|------|-----------|------------------------------|-------|-----|-------|----------|-------------------|
| APSH | Internal | Fac Cal. Vs. Single-point | 27.5 | 1 | 27.5 | 4.96E+04 | < 0.001 |
| | | Error | 0.225 | 406 | 0.001 | | |
| | | Total | 27.7 | 407 | | | |
| APSH | External | Fac Cal. Vs. Single-point | 0.681 | 1 | 0.681 | 536 | < 0.001 |
| | | Error | 0.516 | 406 | 0.001 | | |
| | | Total | 1.19 | 407 | | | |
| APSH | Internal | Factory Cal. vs. Multi-point | 28.3 | 1 | 28.3 | 6.19E+04 | < 0.001 |
| | | Error | 0.185 | 406 | 0.001 | | |
| | | Total | 28.5 | 407 | | | |
| APSH | External | Factory Cal. vs. Multi-point | 0.692 | 1 | 0.692 | 539 | < 0.001 |
| | | Error | 0.521 | 406 | 0.001 | | |
| | | Total | 1.21 | 407 | | | |
| APSH | Internal | Single-point vs. Multi-point | 0.005 | 1 | 0.005 | 15.0 | < 0.001 |
| | | Error | 0.143 | 406 | 0.000 | | |
| | | Total | 0.148 | 407 | | | |
| APSH | External | Single-point vs. Multi-point | 0.000 | 1 | 0.000 | 0.040 | 0.843 |
| | | Error | 0.415 | 406 | 0.001 | | |
| | | Total | 0.415 | 407 | | | |

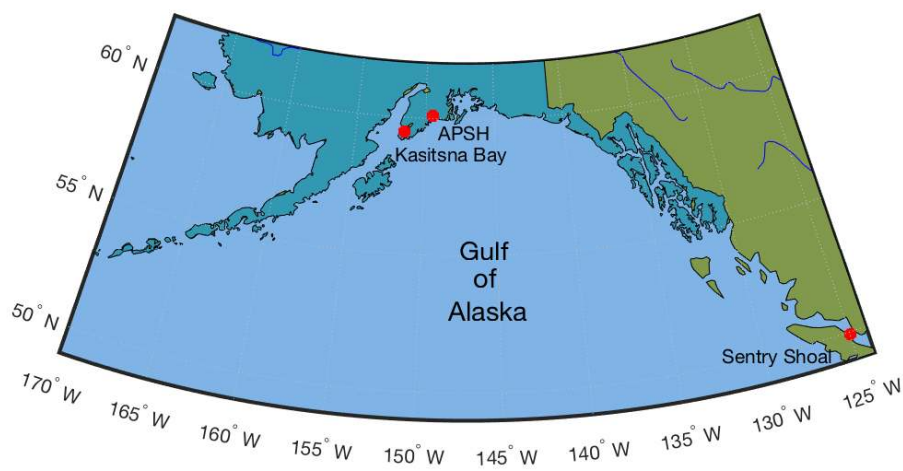
912
 913
 914
 915
 916
 917
 918
 919
 920
 921
 922
 923
 924
 925
 926
 927
 928
 929
 930
 931
 932
 933
 934
 935
 936



937 **Figure 1.**

938

939



940

941

942 Geographical map with locations of SeaFET™ field deployments along Alaska's, USA, south-
943 central coast and one location in the Strait of Georgia, British Columbia, Canada.

944

945

946

947

948

949

950

951

952

953

954

955

956

957

958

959

960

961

962

963

964

965

966

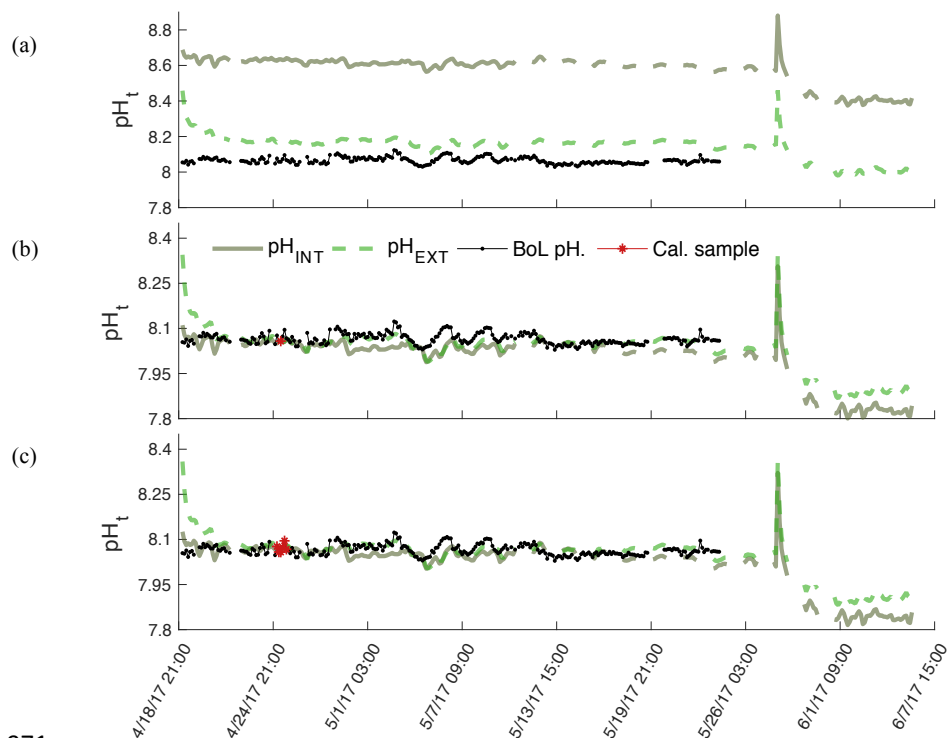
967

968



969 **Figure 2.**

970



971

972

973 pH_t recorded by the internal (solid) and external (dashed) electrodes on SeaFETTM₃₉₇ deployed in
974 parallel with the BoL at the Alutiiq Pride Shellfish Hatchery. pH_t from both electrodes is shown
975 when derived using factory calibration (FC) coefficients (panel a), *in situ* single-point (SC)
976 calibration coefficients (panel b), and *in situ* multi-point (MC) calibration coefficients (panel c).
977 Black solid line is pH_t derived from continuous pCO_2 measurements recorded by the BoL and
978 derived TA from the TA-S relationship (Evans et al. 2015). Red circles are the calibration points
979 from the BoL data.

980

981

982

983

984

985

986

987

988

989

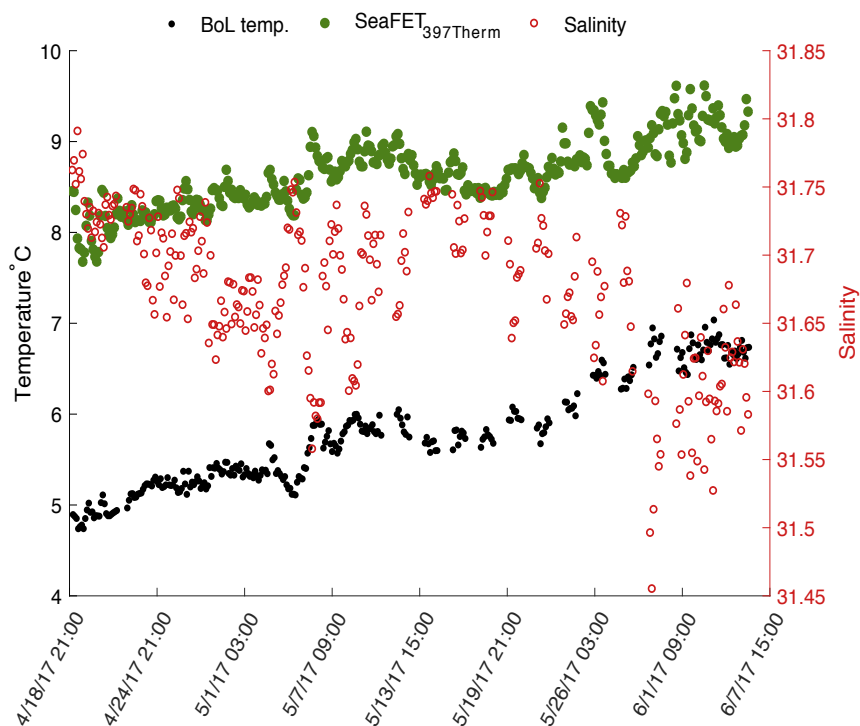
990

991

992



993 **Figure 3.**
994

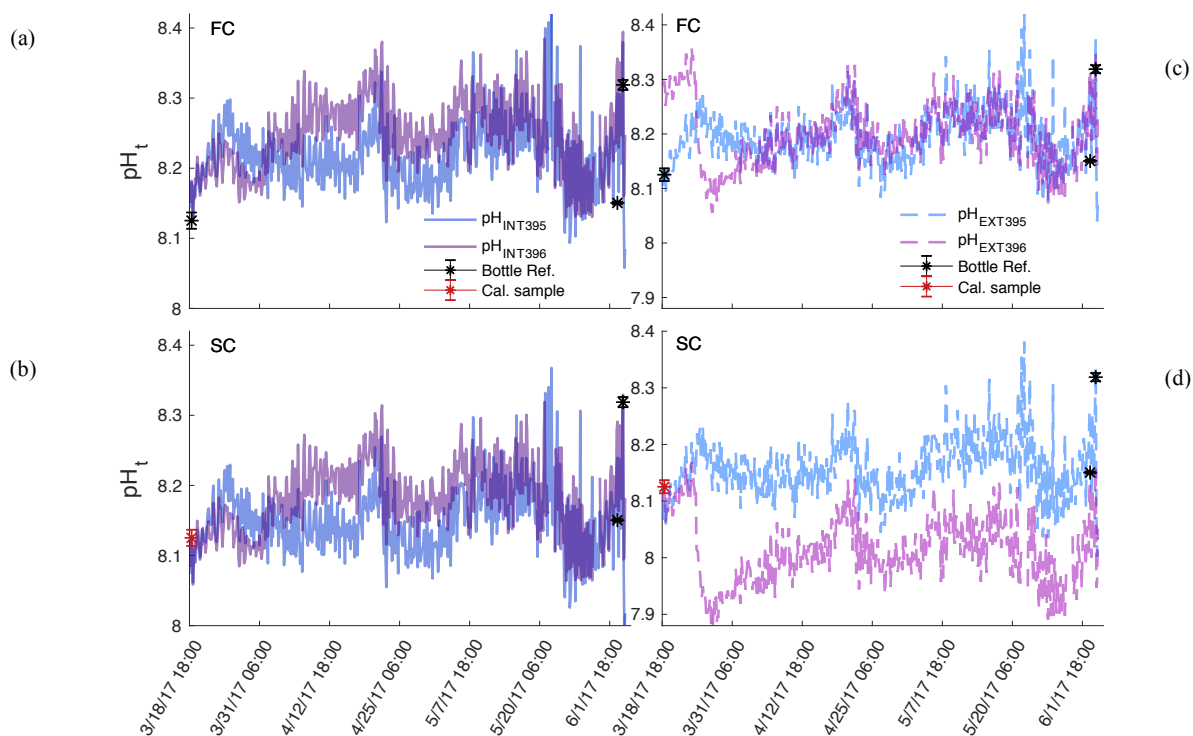


995
996
997
998
999
1000
1001
1002
1003
1004
1005
1006
1007
1008
1009
1010
1011
1012
1013
1014
1015
1016

Temperature derived from the internal thermistor on SeaFETTM₃₉₇ (green circles) and the temperature recorded by the BoL (black circles) at the Alutiiq Pride Shellfish Hatchery from late winter through spring 2017. Salinity (red circles) recorded by the BoL on the right y-axis.



1017 **Figure 4.**
1018



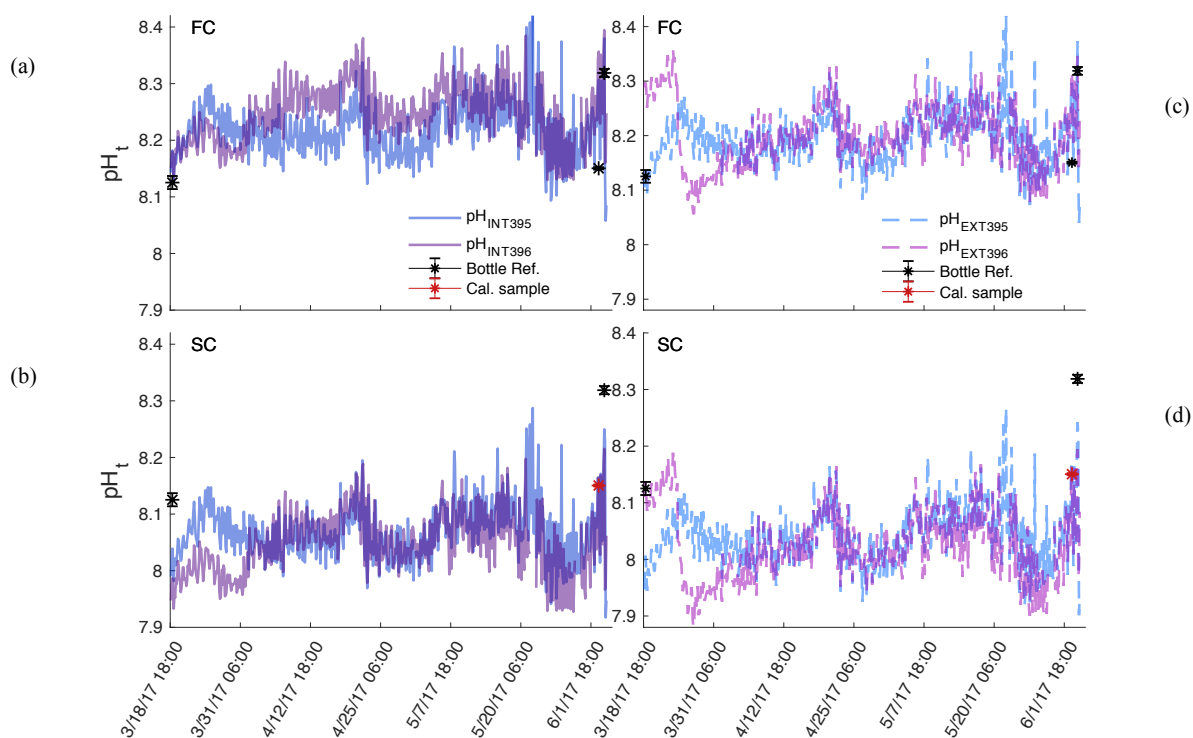
1019
1020
1021
1022
1023
1024
1025
1026
1027
1028
1029
1030
1031
1032
1033
1034
1035
1036
1037
1038
1039

Comparison of pH_t recorded by the internal (panel a and b) and external (panel c and d) electrodes on SeaFETTM₃₉₅ (blue) and SeaFETTM₃₉₆ (purple) before they were conditioned to the environment (non-conditioned) deployed in Kasitsna Bay, AK, based on calibration method: factory calibration (FC) and *in situ* single-point (SC) calibration. Discrete reference samples (black asterisks) and calibration sample (red asterisks) were collected 36 and 12 h pre-SeaFETTM recovery, and < 24 h post-deployment, respectively. Temperature and salinity measurements collected on reference and calibration samples were used to derive SeaFETTM pH_t at those given time points. All other SeaFETTM pH_t measurements use thermistor temperature and salinity logged by Kasitsna Bay data sonde.



1040
1041
1042

Figure 5.

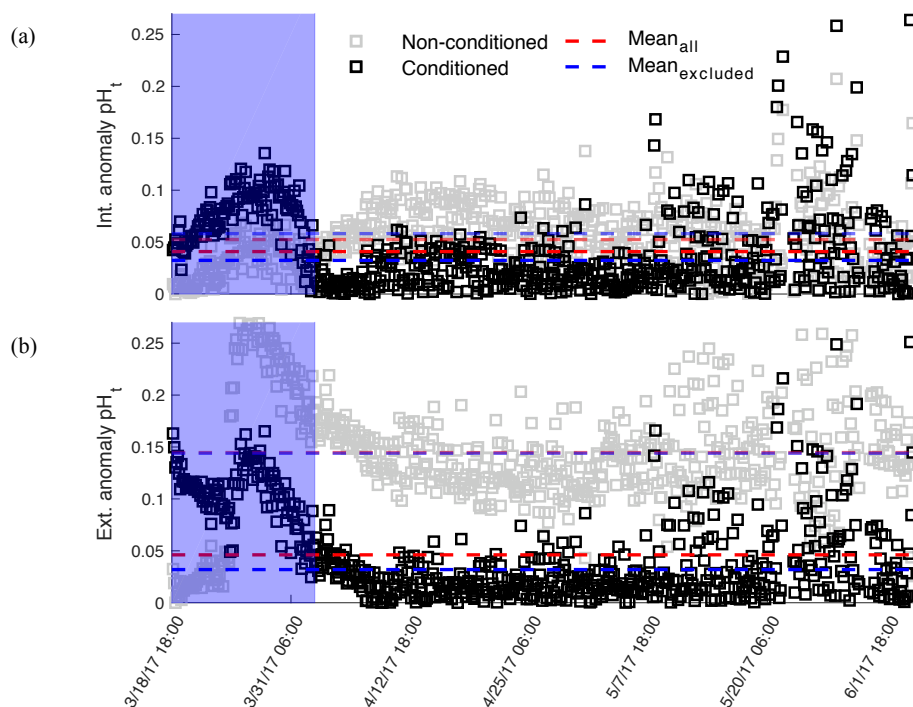


1043
1044
1045
1046
1047
1048
1049
1050
1051
1052
1053
1054
1055
1056
1057
1058
1059
1060
1061
1062

Comparison of pH_t recorded by the internal (panel a and b) and external (panel c and d) electrodes on conditioned SeaFETTM₃₉₅ (blue) and SeaFETTM₃₉₆ (purple) deployed in Kasitsna Bay, AK, based on calibration method: factory calibration (FC) and *in situ* single-point (SC) calibration. Discrete reference samples (black asterisks) and calibration sample (red asterisks) were collected < 24 h post deployment and 12 h pre-SeaFETTM recovery, while calibration sample was collected 36 h pre-SeaFETTM recovery. Temperature and salinity measurements collected on reference and calibration samples were used to derive SeaFETTM pH_t at those given time points. All other SeaFETTM pH_t measurements use thermistor temperature and salinity logged by Kasitsna Bay data sonde.



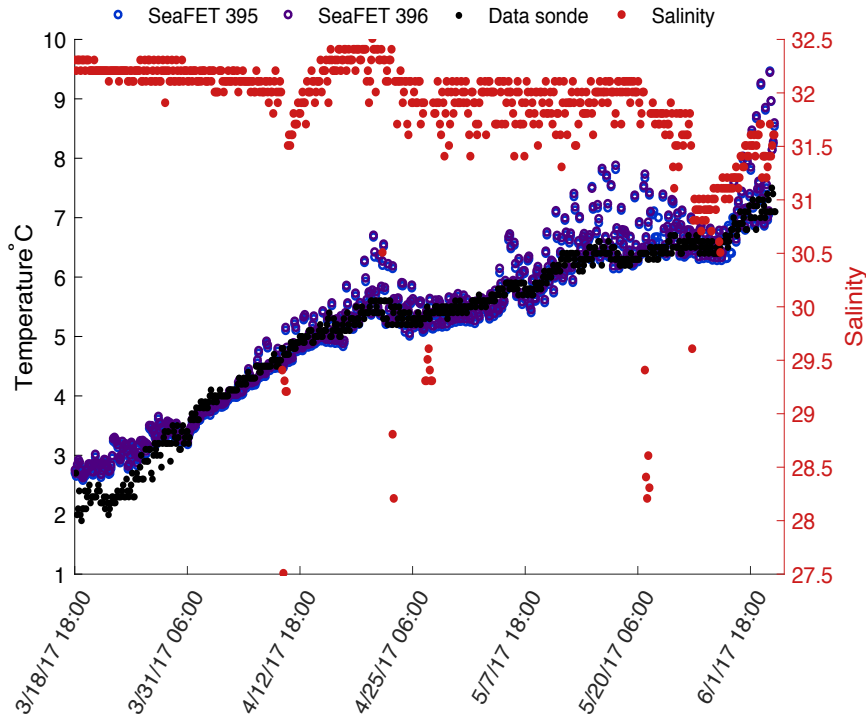
1063
1064 **Figure 6.**
1065



1066
1067
1068 Mean pH_t anomaly between *in situ* single-point calibrated SeaFETTM₃₉₅ and SeaFETTM₃₉₆
1069 internal (panel a) and external (panel b) electrodes during parallel deployment in Kasitsna Bay,
1070 AK. Intra-anomaly comparison based on calibration sample taken at initial deployment (< 24 h
1071 non-conditioned, gray squares) and end of deployment (36 h pre-recovery, black squares).
1072 Shaded blue region indicates conditioning period. Data points in blue region omitted when mean
1073 anomaly was calculated (non-conditioned: transparent blue-dashed line; conditioned: bold blue-
1074 dashed line) compared to mean anomaly from entire data set (non-conditioned to environment:
1075 red-dashed line; conditioned: red- dashed line).
1076
1077
1078
1079
1080
1081
1082
1083
1084
1085
1086



1087
1088 **Figure 7.**
1089

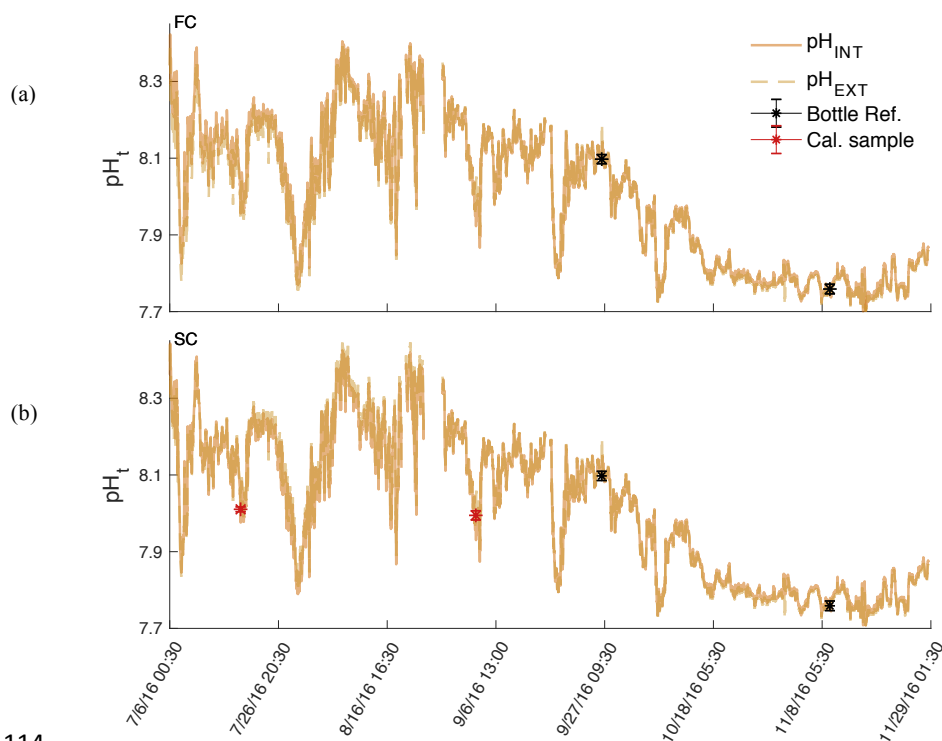


1090
1091
1092 Temperature derived from the internal thermistor on SeaFETTM₃₉₅ (blue) and SeaFETTM₃₉₆
1093 (purple) compared against the temperature recorded by the Kachemak Bay National Estuarine
1094 Research Reserve data sonde. Salinity (Red circles) recorded by Kachemak Bay data sonde on
1095 the right y-axis.

1096
1097
1098
1099
1100
1101
1102
1103
1104
1105
1106
1107
1108
1109
1110



1111
1112 **Figure 8.**
1113



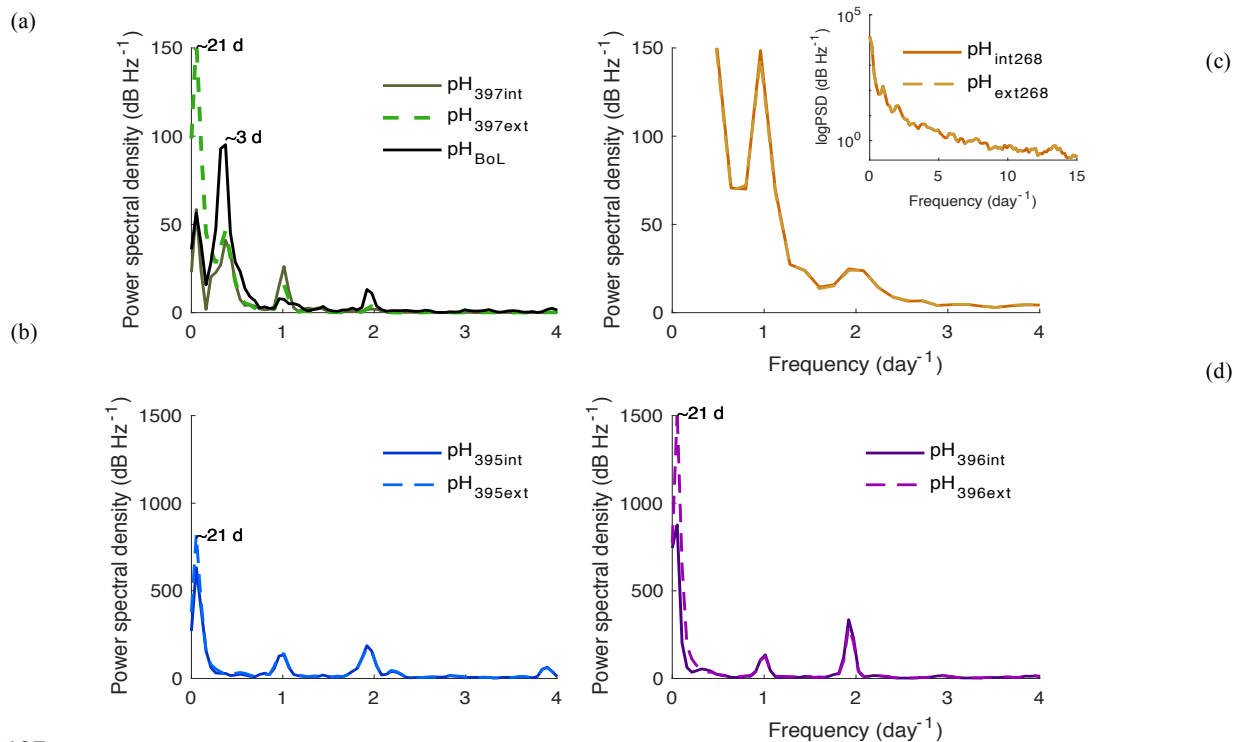
1114
1115
1116 pH_t recorded by the internal (solid) and external (dashed) electrodes on SeaFETTM₂₆₈ deployed at
1117 the Sentry Shoal mooring. pH_t from both electrodes is shown when derived using factory
1118 calibration (FC) coefficients (panel a) and *in situ* single-point (SC) calibration coefficients (panel
1119 b). Black asterisks are references samples taken after initial calibration and recalibration (red
1120 asterisk), where pH_t was derived from TCO_2 and pCO_2 measurements made on the BoL at the
1121 Hakai Institute's Quadra Island Field Station.

1122
1123
1124
1125
1126
1127
1128
1129
1130
1131
1132
1133
1134



1135 **Figure 9.**

1136



1137

1138

1139 Power spectral density (PSD) analysis of pH_t in frequency per day for SeaFETs™ 397 (panel a),

1140 268 (panel b), 395 (panel c), and 396 (panel c). Inset in panel b is log base 10 transformed PSD

1141 analysis of same data set. All internal electrodes marked as solid colored lines while external

1142 electrodes are colored dashed lines. BoL data set marked as solid black line (panel a).

1143

1144

1145

1146

1147

1148

1149

1150

1151

1152

1153

1154

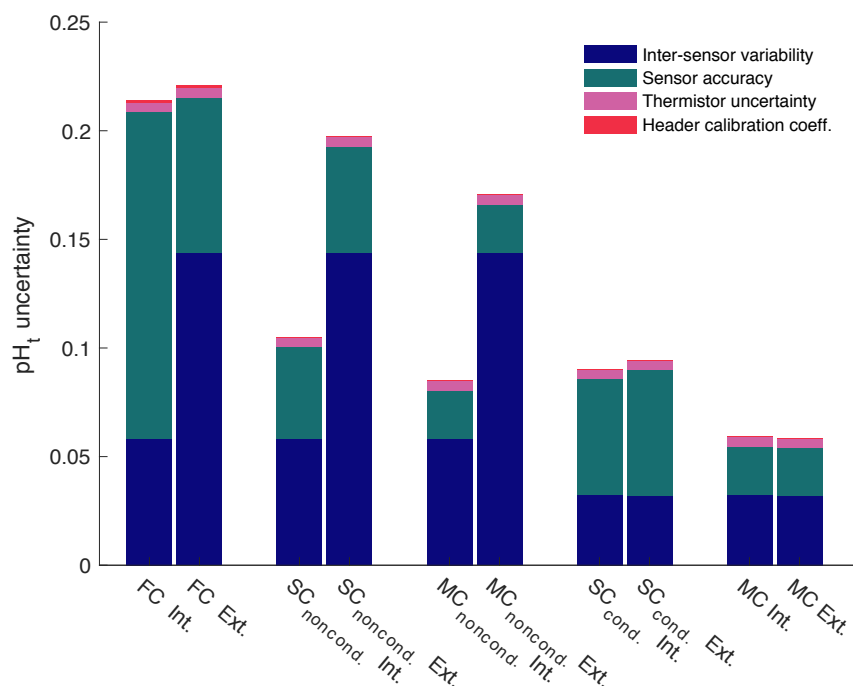
1155

1156

1157



1158 **Figure 10**
 1159



1160
 1161
 1162
 1163
 1164
 1165
 1166
 1167
 1168
 1169
 1170
 1171
 1172
 1173
 1174
 1175
 1176

Quantified uncertainties based on field deployments of all Sea-Bird SeaFETsTM separated by electrode calibration method (FC: factory; SC: single-point; MC: multi-point), and calibration time for SeaFETsTM 395 and 396 (i.e., non-conditioned to environment and conditioned). pH_t accuracy uncertainty calculated as the mean difference when comparing the absolute difference between reference samples and SeaFETsTM 395 (non-conditioned to environment and conditioned), 396 (non-conditioned to environment and conditioned), and 268 as well as the average absolute difference between SeaFETTM 397 and the BoL. Inter-sensor variability uncertainty determined by comparing SeaFETsTM 395 (non-conditioned to environment and conditioned) and 396 (non-conditioned to environment and conditioned), deployed side-by-side in Kasitsna Bay. Thermistor uncertainty is calculated pH_t error when using thermistor derived temperature rather than external temperature sensor determined from SeaFETsTM 395 and 396. Header calibration coefficient uncertainty is the discrepancy in pH_t when using SeaFETcom factory calibration coefficients from header file rather than disc file.